DISCLAIMER

This report was prepared as an account of work sponsored by an agency of the United States Government. Neither the United States Government nor any agency thereof, nor any of their employees, makes any warranty, express or implied, or assumes any legal liability or responsibility for the accuracy, completeness, or usefulness of any information, apparatus, product, or process disclosed, or represents that its use would not infringe privately owned rights. Reference herein to any specific commercial product, process, or service by trade name, trademark, manufacturer, or otherwise does not necessarily constitute or imply its endorsement, recommendation, or favoring by the United States Government or any agency thereof. The views and opinions of authors expressed herein do not necessarily state or reflect those of the United States Government or any agency thereof. Reference herein to any social initiative (including but not limited to Diversity, Equity, and Inclusion (DEI); Community Benefits Plans (CBP); Justice 40; etc.) is made by the Author independent of any current requirement by the United States Government and does not constitute or imply endorsement, recommendation, or support by the United States Government or any agency thereof.

ORNL/SPR-2025/4182

High-Burnup BWR LOCA Burst Analysis Using High-Fidelity Multiphysics Simulations

Ian Greenquist
Aaron Wysocki
Nathan Capps
Mehdi Asgari
Shane Henderson
Robert Salko
Ian Porter
Guangjun Li
Baris Sarikaya

September 2025

OAK RIDGE National Laboratory

ORNL IS MANAGED BY UT-BATTELLE LLC FOR THE US DEPARTMENT OF ENERGY

ORNL/SPR-2025/41822025/4182

Nuclear Energy Advanced Modeling and Simulation

High-Burnup BWR LOCA Burst Analysis Using High-Fidelity Multiphysics Simulations

Ian Greenquist[1]
Aaron Wysocki[1]
Nathan Capps[1]
Mehdi Asgari[1]
Shane Henderson[1]
Robert Salko[1]
Ian Porter[2]
Guangjun Li[2]
Baris Sarikaya[3]

1. Oak Ridge National Laboratory
2. General Electric Vernova
3. Constellation Nuclear

September 2025

Prepared by
OAK RIDGE NATIONAL LABORATORY
Oak Ridge, TN 37831
managed by
UT-BATTELLE LLC
for the

US DEPARTMENT OF ENERGY
under contract DE-AC05-00OR22725

CONTENTS

LIST OF FIGURES

ABBREVIATIONS

ADS	automatic depressurization system
BWR	boiling water reactor
CC	Chapman correlation
CS	Core spray
FFRD	fuel fragmentation, relocation, and dispersal
FGR	fission gas release
HBLUA	high-burnup lead use assembly
HPCI	high-pressure coolant injection
INL	Idaho National Laboratory
LBLOCA	large-break loss-of-coolant accident
LOCA	loss-of-coolant accident
LHR	linear heat rate
LPCI	low-pressure coolant injection
LWR	light water reactor
NEAMS	Nuclear Energy Advanced Modeling and Simulation
ORNL	Oak Ridge National Laboratory
PBCC	point-biserial correlation coefficient
PCT	peak cladding temperature
PFT	peak fuel temperature
PWR	pressurized water reactor
SBLOCA	small-break loss-of-coolant accident
SRC	strain rate criterion
TRACE	TRAC/RELAP Advanced Computational Engine
VERA	Virtual Environment for Reactor Applications

ABSTRACT

The US nuclear industry is looking to improve on the operating economics of the current fleet of light-water reactors (LWRs). One way of achieving this is by operating fuel to higher burnup. In pressurized water reactors (PWRs), relaxing the current burnup limit will allow for cycle length extensions and power uprates; in boiling water reactors (BWRs) it may allow for improved fuel utilization and reduced feed assemblies, as well as more efficient power uprates and increased capacity factors that will support the Administration's Executive Order to facilitate 5 GW of power uprates at existing nuclear facilities. However, one of the key limitations to operating fuel to higher burnup is the risk of fuel fragmentation, relocation, and dispersal (FFRD). Recognizing the high interest in extending burnup limits, the US Nuclear Regulatory Commission (NRC) has issued Draft Regulatory Guide DG-1434, which defines an approach that would be acceptable to the NRC for addressing FFRD risk. The approach defined will require better understanding of the phenomena leading to FFRD as well as best-estimate simulation methods to understand FFRD risk in high-burnup cores.

The Nuclear Energy Advanced Modeling and Simulation program is supporting the FFRD industry challenge problem through development of state-of-the-art, high-fidelity modeling and simulation LWR analysis capabilities; namely, the BISON fuel performance code and the VERA core simulator software. These tools, along with the US NRC TRACE system analysis code, have been utilized for analysis of FFRD risk in both PWR and BWR cores in recent years. The work documented in this report addresses the lack of high-fidelity research for BWRs and builds on a previous activity where the framework has been applied to Cycles 16 through 18 of Limerick Unit 1, a BWR/4, with introduction of 8 high-burnup lead use assemblies (HBLUAs) that were representative of the 8 HBLUAs loaded into Limerick Unit 2 in 2021. VERA was used in this previous activity to model rod-by-rod depletion in these cycles, and its solution was used to initialize a TRACE simulation of a large-break loss-of-coolant accident (LBLOCA) at the end of Cycle 18.

In the work documented in this report, the TRACE model was improved by refining the core mesh and utilizing a new feature that allows for capturing the full 3D VERA power distribution in the model. This allows for a more detailed solution for setting BISON boundary conditions. Furthermore, the solutions from VERA and TRACE were used to set up and perform BISON simulations of about 1,000 rods sampled from the core, including all burnup levels. Utilizing two cladding burst models, it was shown that no fuel rods were predicted to burst during the postulated LBLOCA transient. Additionally, a sensitivity study was performed by artificially increasing linear heat rate during the postulated LBLOCA to identify parameters that correlate with rod burst susceptibility. Burnup, fission gas release, and hoop strain were all found to be positively correlated with rod burst susceptibility. Small-break loss-of-coolant accident (SBLOCA) analyses were also performed; these analyses predicted cladding temperature increases that were bounded by the LBLOCA cladding temperatures for all small break sizes studied for this plant. However, future refinements to the plant response assumptions during the SBLOCA could impact the predicted cladding response. Finally, a benchmark study was performed between CTF and TRACE for LOCA conditions to better qualify CTF for BWR LOCA modeling.

1. INTRODUCTION

In an effort to reduce costs and improve efficiency, the nuclear energy industry is pushing to expand the operational envelope of the existing fleet. Operating the fuel to a higher burnup is a potential approach for improving fuel utilization and reducing feed assemblies, which will improve fuel cycle economics. The Nuclear Energy Advanced Modeling and Simulation (NEAMS) program is supporting this effort by developing high-fidelity computational tools that can predict fuel and reactor performance in pressurized water reactors (PWRs) and boiling water reactors (BWRs). As part of this effort, a multiphysics code-

coupling framework has been developed to model high-burnup large-break loss-of-coolant accidents (LOCAs) and predict the cladding ballooning and burst behavior and, subsequently, FFRD susceptibility. The framework was originally applied to PWRs [1–4] but has since been expanded to include BWRs [5,6]. However, a full-core analysis of cladding balloon and burst and FFRD susceptibility of a BWR has not been accomplished using the framework. The purpose of this work is to expand the number of rods included in the transient analysis and obtain a statistically representative estimation of the full-core FFRD susceptibility of the Limerick Unit 2 BWR core during a postulated large-break LOCA (LBLOCA).

Current core designs are limited to an initial enrichment limit of 5% and a peak average burnup limit of 62 GWd/MTU ultimately constraining core designs and leading to increased fuel cycle costs. Relaxing these constraints enables more efficient core designs, improves fuel utilization, reduces reload batch fractions and hence spent fuel storage requirements, and consequently reduces the fuel cycle cost. In the meantime, implementation challenges for the safety analyses need to be better understood and addressed. Namely, the tendency of oxide fuels to crack and fragment during operation, as well as the risk of release during design basis accidents that can cause fuel ballooning and rupture, must be better understood. The nuclear energy industry, universities, national laboratories, and regulators are working together to improve our collective understanding of operating LWR fuel beyond the currently established burnup and enrichment limits.

However, achieving these goals requires advanced tools that can accurately predict the plant and fuel responses. This work is part of an effort to better understand and predict, and if observed, minimize, prevent, or mitigate the consequences of FFRD in BWRs. High-fidelity tools may provide a better understanding of how neutron transport, thermal hydraulics (T/H), fuel performance, transient response, and feedback effects contribute to FFRD throughout the entire core region and operating history by more accurately modeling local burnup, fuel fragmentation, fission gas release, and their impact on cladding rupture and fuel release during limiting transients.

This milestone documents a comprehensive high-fidelity multiphysics analysis to model a BWR core during a LOCA. The proposed method coupled VERA, TRACE, and BISON to obtain high-fidelity, rod-specific predictions throughout a core depletion and during a LOCA transient for all the high-burnup fuel rods. Section 2 summarizes the multiphysics code coupling framework. Section 3 describes the BWR model used for the simulation and conditions specific to the operating cycles being modeled. Section 4 describes transient T/H simulations of the LOCA using TRACE. Section 5 applies the results of the T/H simulations as boundary conditions in fuel performance simulations and calculates the likely FFRD susceptibility. Section 6 describes a sensitivity and uncertainty study used to quantify the effects of LHR uncertainty on the FFRD predictions. Finally, Section 7 presents a benchmark comparison between CTF, the subchannel T/H code in VERA, and TRACE for LOCA in a BWR to investigate the impact of rod-resolved modeling on results. Conclusions are drawn and future work is proposed in Section 8.

2. MULTIPHYSICS CODE-COUPLING FRAMEWORK

The multiphysics code-coupling framework used in this work is shown in Figure 1. It includes three codes. First, VERA simulates the reactor core during multiple cycles. VERA is a full-core, rod-resolved, high-fidelity multiphysics solver used for analyzing LWR cores. VERA boasts several advanced capabilities that facilitate high-fidelity high-burnup depletion simulations, including rod-resolved isotopic and reaction distributions and thermal feedback. VERA's neutronic and subchannel modules allow local feedback effects to be captured accurately within the fuel rod power distributions that could form the basis of the fuel performance calculations performed by BISON. This approach forms the basis of the multiphysics framework.

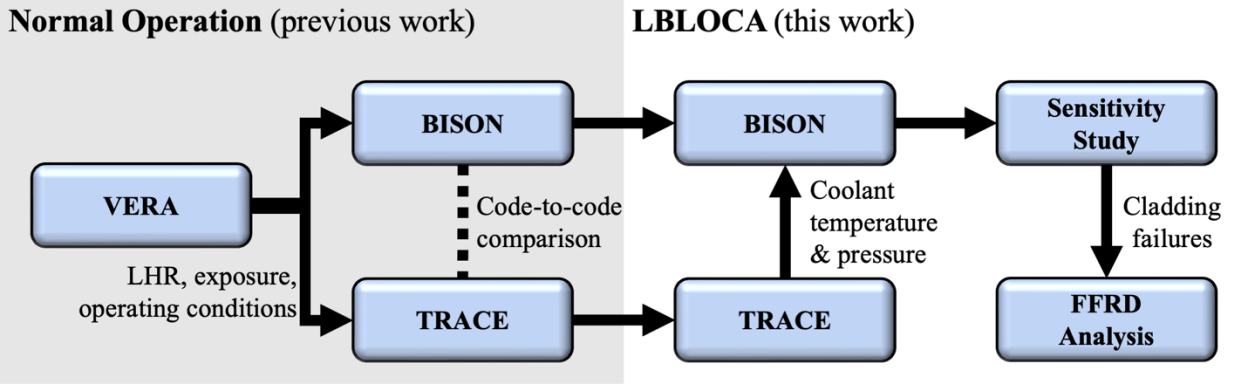

Figure 1. Visualization of the multiphysics code coupling strategy used in this work. The normal operation portion of the strategy was documented in a previous report [5].

In October 2019, DOE-NE funded a two-year project entitled "Modeling and Analysis of Exelon BWRs for Eigenvalue & Thermal Limits Predictability." The primary objective of this project was to enhance VERA's capabilities to support detailed modeling and simulation of BWRs. During the two-year development period, tremendous progress was made, but the project did not achieve full BWR VERA capability development with application demonstration. The benchmarking of 15 cycles showed promising results but identified multiple additional development areas such as refined axial rod power distribution predictions at certain portions of the cycles. When compared with the measured data from in-core detectors, errors as high as 15% were observed around the middle of cycles [5]. Further development is needed to identify the root causes of such mispredictions to improve VERA prediction ability. Although VERA is not fully matured for consistent and accurate prediction of BWR performance, the overall high-fidelity simulation infrastructure was successfully developed.

TRACE is an NRC T/H system code for best estimate analyses of steady-state and transient reactor behavior, building on TRAC-P, TRAC-B, RELAP5, and RAMONA [7]. It solves a six-equation formulation including mass, momentum, and energy conservation equations for the liquid and vapor phases. It is applicable to a wide range of nuclear reactor types including PWRs, BWRs, and advanced reactors. Its qualification basis includes validation against separate-effects and integral LOCA testing, showing that it adequately predicts LOCA behavior across all postulated break sizes and conditions.

The BISON fuel performance code is a finite-element-based thermomechanical analysis tool maintained at INL and developed through a collaborative framework by a variety of laboratories, universities, and private institutions [8]. BISON uses a flexible, modular design that allows it to be used for a wide array of fuel and cladding types. It contains models for a wide range of nuclear fuel-specific effects such as cladding ballooning, fission gas generation and release, and irradiation hardening, to name a few. BISON has a robust validation database that includes both PWR and BWR data. However, some BWR-specific capabilities (e.g., cladding liners) have been missing from BISON's modeling capabilities. Recent updates have included some of these features [9], but at the time of this work those capabilities had not yet been fully implemented and were not used in this work.

The code VERAOneWay was used to populate a BISON input file template with rod-specific normal operation data from VERA. The results of those simulations have been previously published [5,6]. LOCA data from TRACE were then appended to the existing BISON simulations to create fuel performance simulations that included the full power history of the rods, including the LOCA.

3. LIMERICK UNIT 1 CORE AND CYCLE DESIGN

The core model for Limerick was documented in the FY24 milestone report [5]. To recap, Limerick Unit 1 is a General Electric BWR-4 that started operation in 1986. A high-burnup core was simulated by inserting high burnup lead use assemblies (HBLUAs) in the core and shuffling them through three cycles of operation (Cycles 16 through 18). In reality, the HBLUAs were operated in Limerick Unit 2 [10]; however, the VERA model is developed for Unit 1, so the HBLUAs were artificially placed in the same locations as they were located in Unit 2. The HBLUAs were pushed beyond the typical peak burnup to simulate BWR high-burnup operating conditions in order to analyze cladding balloon and burst behavior and FFRD susceptibility. Figure 2 shows the burnup in each bundle at start of Cycle 18, with the HBLUA bundles identified.

Table 1 provides a summary of the rod burnup for the HBLUAs at the end of the last cycle, as predicted by VERA.

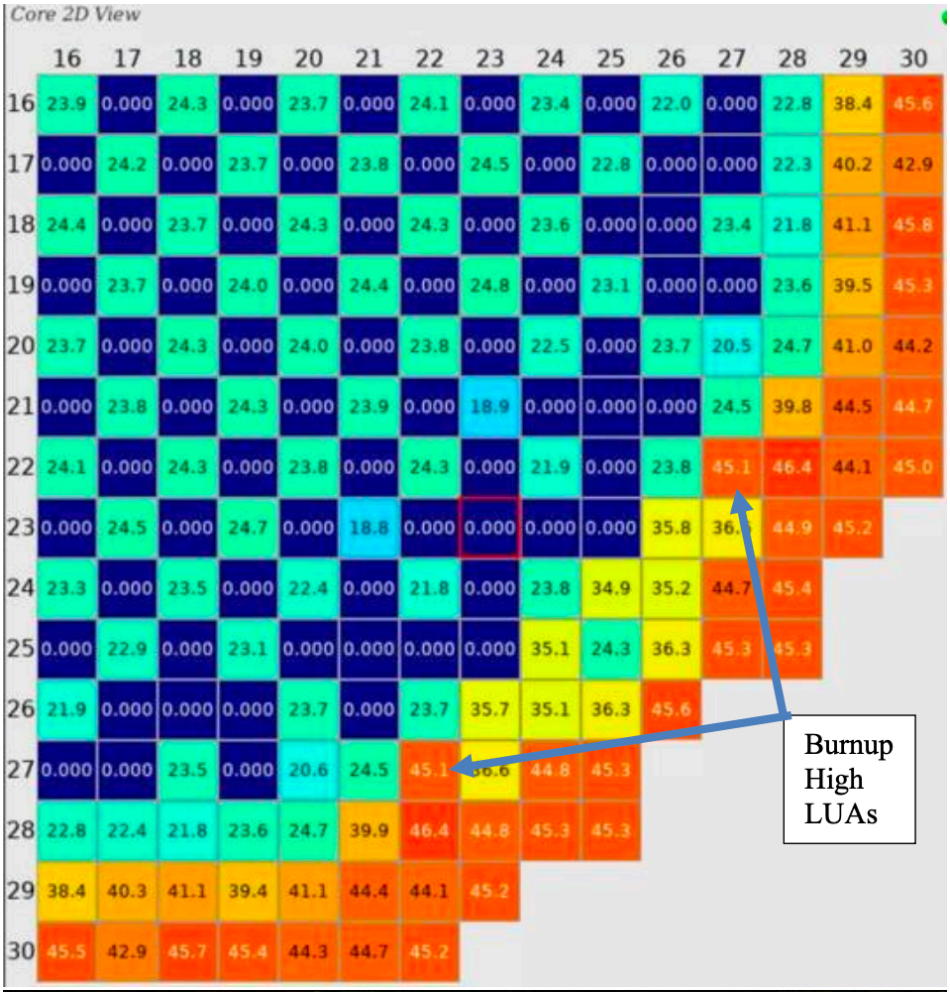

Figure 2. Bundle average burnup at beginning of Cycle 18 with HBLUA locations marked.

Table 1. Calculated burnup data for HBLUAs

	Beginning of Third Cycle			End of Third Cycle		
Assembly Location	Assembly avg. burnup (GWd/MTU)	Max. 2D rod avg. burnup (GWd/MTU)	Peak pellet exposure (GWd/MTU)	Assembly avg. burnup (GWd/MTU)	Max. 2D Rod avg. burnup (GWd/MTU)	Peak pellet exposure (GWd/MTU)
27-22	45.08	51.77	60.60	55.78	64.61	72.90
22-27	45.11	51.78	60.60	55.82	64.66	72.90

The benchmarking of 15 cycles with VERA showed promising results but revealed multiple issues and inconsistent prediction of the axial pin power distributions at certain portions of the cycles. When compared with the measured data from traversing in-core probe (TIP) detectors, the 3D RMS ranged from 5% for many points in the cycle to unacceptable levels of 15% at and around the middle of cycles. VERA tends to underpredict the axial power peak in the bottom of the core. The cause for these unacceptable predictions is unknown, and further investigations and developments are needed to identify the root causes of such mispredictions to improve VERA prediction ability. Although VERA is not yet fully matured for consistent and accurate prediction of BWR performance, the overall high-fidelity simulation infrastructure was successfully developed.

The VERA depletion model was not modified from the FY24 model, so results used in the TRACE and BISON analyses are the same. However, it should be noted that a post-processing script was developed to collect and reformat VERA solution data into a format that could be used by GNF for benchmarking activities. In addition to reformatting the solution data, it was also necessary to add additional model information such as rod enrichment, bundle residence time, bundle product type, and rod gadolinia content. This was all populated into an agreed upon format in an HDF5 file for all three cycles and delivered to GNF for future benchmarking purposes.

4. TRACE TRANSIENT ANALYSIS

4.1 BACKGROUND

TRACE was applied previously to a high-burnup LOCA in a Westinghouse 4-loop PWR, using VERA depletion results for 281 rods [1]. Steady-state fuel temperatures predicted by TRACE agreed with BISON, and the LOCA model—based on the BEMUSE large-break LOCA benchmark with 3D vessel/core representation and other improvements—provided boundary conditions for BISON rod burst analyses and experimental design.

In FY24, this work was extended to BWRs, using VERA depletion for Limerick to define high-burnup rod conditions and perform a preliminary steady-state and transient analysis in TRACE, generating boundary conditions for BISON. That preliminary study was limited to an 8-channel representation of the core. Four of the channels represented individual assemblies of interest, while the remaining four channels were lumped channels representing the remainder of the core. The four individual assembly channels represented a range of bundle power and burnup levels, including assemblies taken from different reload batches in the cycle. A single rod approximating the hot rod was modeled individually within each of these assemblies, with the remaining rods in the assembly modeled as an additional lumped rod. Certain aspects of the part-length rods were modeled in this approach while other aspects were approximated. Specifically, the change in flow area and hydraulic diameter due to part-length rods is directly accounted for in the TRACE channel thermal hydraulic model. However, for simplicity in setting up the solid heat conduction calculation, all fuel rods were treated as full-length rods, but with zero power applied to the axial levels where the physical rod is absent. Although more fuel mass was modeled in this approach than was realistic, the approach still ensured that the correct total power (W) was generated at

each axial level in the average power rod group, consistent with VERA. This may have impacted the average rod cladding temperature behavior; however, only the cladding temperatures in the 945 individual rods of interest were assessed in this study, and these should not be significantly impacted by this approach. More precise treatment of partial rod lengths may be investigated in the future, however, as time permits.

The TRACE code version that was available at the time, TRACE 5.0 Patch 7, did not allow detailed rod-by-rod specification of axial powers. Instead, a single axial power shape can be specified and applied to all rods in the assembly, scaled by a scalar multiplier on rod power to approximate the power values in a given rod of interest.

In FY25, TRACE 5.0 Patch 9 was obtained, which allows full flexibility to specify unique axial power distributions in each of the rods to capture both the rod average power and the axial power shape variations from rod to rod. The axial burnup distribution is modeled individually for each rod in a similar fashion.

As discussed in Section 5, several individual fuel rods from each of the quarter-core assemblies were modeled in BISON to predict the rods' steady state and transient LOCA behavior. This included a total of 945 fuel rods throughout the quarter core. Another key improvement to the FY25 TRACE analyses was to model each of these 945 rods explicitly within the TRACE simulation. This involved modeling all of the assemblies in the quarter core individually, rather than restricting the analysis to four selected individual assemblies along with representative combined channel modeling. It also required automatically identifying which of the rods in each assembly were modeled in BISON and then extracting their locations, axial power distribution, and axial burnup distribution and writing them to the TRACE input deck. A set of Python scripts was developed to perform these steps in order to automate the process of spawning TRACE channels, defining the appropriate fuel rod groups, and writing the appropriate values.

4.2 SIMULATION SETUP

A TRACE BWR model was developed for this study using an existing TRACE model for a BWR/4 plant. A thorough review confirmed that the model's balance-of-plant (BOP) configuration closely resembles that of Limerick-2. Both systems are BWR/4 plants featuring 764 fuel bundles, which leads to similar sizes and capacities for key components such as the reactor pressure vessel (RPV), recirculation pumps, and emergency core cooling system (ECCS), as well as comparable reactor power and flow rates. Although there may be minor differences in the ECCS and containment setups—meaning the LOCA results might not perfectly replicate Limerick-2's response—the overall behavior is considered reasonably representative for the intended purpose of this work. One noted difference is that the low-pressure coolant injection (LPCI) is actually injected into the core shroud, while in this model, it is injected into the recirculation line. Future work will further refine the model to better match Limerick-2 unit in terms of system response and safety system line-up.

Accordingly, the original BOP configuration and assumptions were maintained, with the following modifications made for Limerick-2:

- A TRACE CHAN component was added to represent the GNF2 fuel type (fuel rods and flow paths in each bundle).
- 195 total CHANs were used, representing 191 individual assemblies in the quarter core and 4 assemblies being averaged assemblies representing the remainder of the core
- The steady-state calculation was set to the Limerick-2 nominal operating power of 3515 MW.
- The post-scram decay power curve was scaled to start at an initial core power of 3515 MW.
- A target core inlet temperature of 551 K was imposed, based on Limerick-2 design parameters.
- A target RPV pressure of 7.24 MPa was applied in line with the design specifications.

- Under a single failure assumption, the ECCS equipment assumed to be operational was: 3 LPCI, 1 core spray (CS), automatic depressurization system (ADS), high pressure coolant injection (HPCI). Note that this is based on a diesel generator failure; a more limiting single failure may be a battery failure in which HPCI is not available. This scenario will be analyzed in future work.

Developing a representative GNF2 TRACE CHAN component required extensive calculations and detailed inputs to accurately capture the GNF2's geometric design and performance characteristics. Although specific proprietary details cannot be disclosed, the model qualitatively incorporates several key design features:

- It properly captures the heated and unheated regions of part-length rods
- It models water rods with explicit simulation of water flow within each TRACE CHAN component.
- It accounts for variations in flow area along the bundle height—caused by the presence of part- and full-length rods and water rods—and includes both reversible and irreversible friction losses from sudden flow area changes.
- It incorporates friction losses (K-factors) from grid spacers, applied at the nearest axial cell edge to each spacer's location.
- It considers inlet orifice friction losses based on each bundle's radial position, using the Limerick-2 inlet orifice map to scale reference K-factors according to the actual inlet flow area.
- It models the channel box surrounding each GNF2 bundle.
- It applies axially dependent hydraulic diameters derived from changes in flow areas and wetted perimeters.

This comprehensive approach ensures the TRACE CHAN component accurately reflects the critical aspects of the GNF2 design.

Figure 3 displays the system diagram of the TRACE model, which incorporates all essential components to realistically simulate a BWR LOCA event. The primary loop spans from the feedwater lines to the steam lines and turbine bypass. Both the drywell and wetwell are included to receive discharge flow during transients and to supply cooling water as needed.

Figure 4 provides a clearer view of the vessel and recirculation loop. Each of the two explicitly modeled recirculation loops includes a recirculation pump, jet pump, LPCI inlet points, and associated piping. The vessel is represented as a three-dimensional cylinder divided into two azimuthal sectors and three radial rings. Each recirculation loop connects to its own azimuthal sector, while the three rings delineate the downcomer and two core regions. Further details on the core layout and bundle configuration are described in a later section.

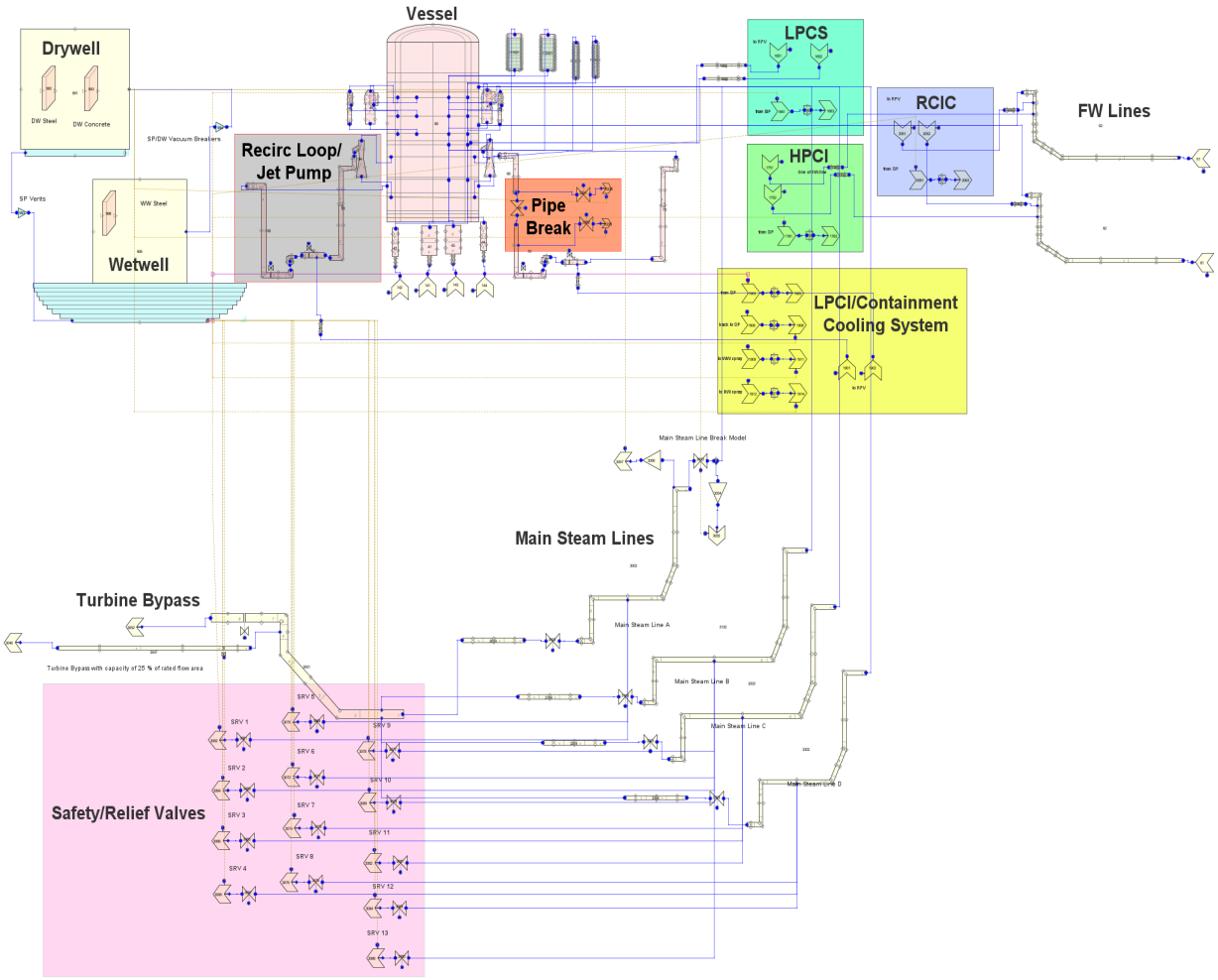

Figure 3. System diagram for the TRACE BWR model.

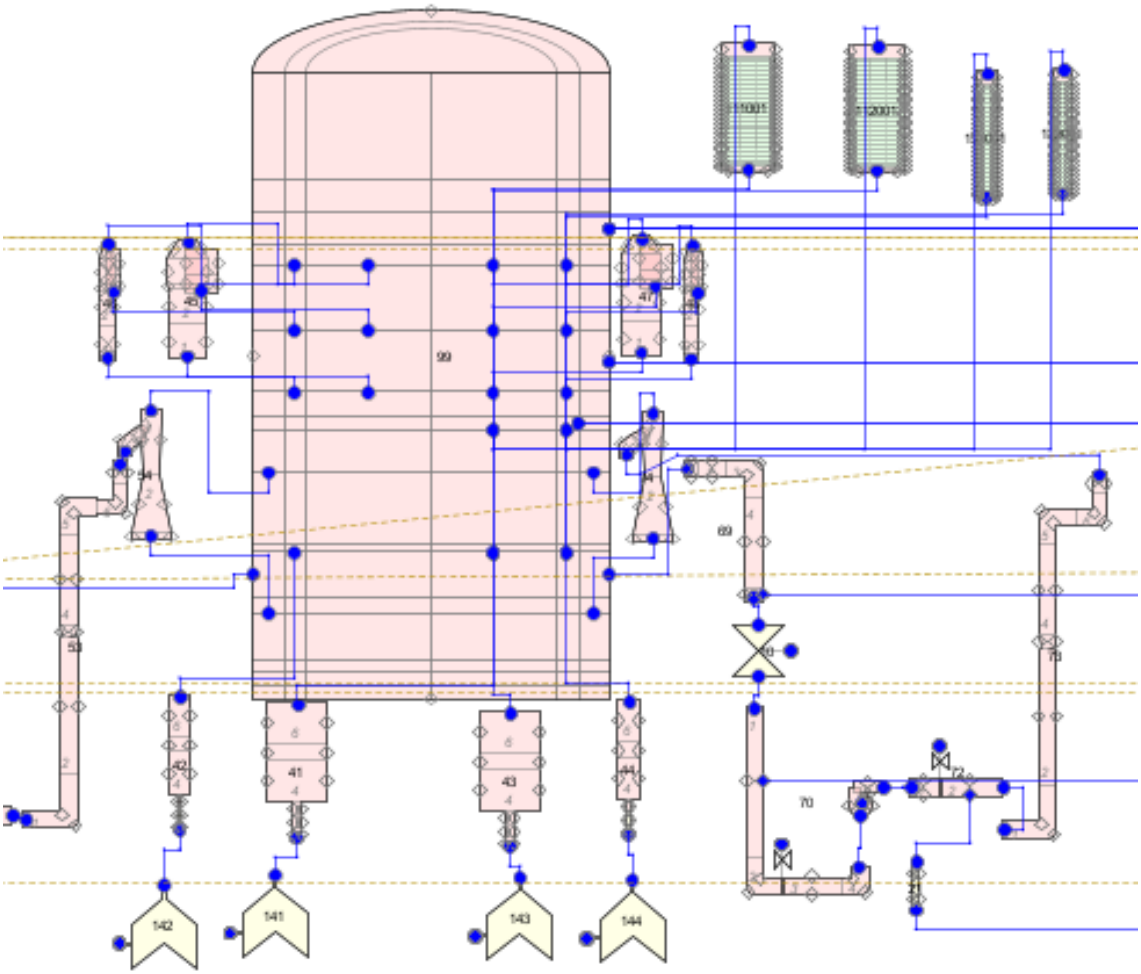

Figure 4. Diagram of the reactor pressure vessel, core channels, recirculation loops, and related components.

Modeled ECCS features include the HPCI, LPCI, LPCS, the suppression pool cooling function of the residual heat removal (RHR) system, the RCIC system, the automatic depressurizations system (ADS), and the condensate storage tank. Each system follows BWR/4 plant specifications with the appropriate ECCS line-up for each diesel generator, proper flow distribution to injection points, setpoint-based actuation (based on RPV water level, system pressure, etc.), and configurable activation delays. These delays can be set to typical LOCA analysis values, accounting for factors such as loss of offsite power (LOOP). Specifically, HPCI, LPCS, and LPCI are triggered by RPV Low Level signals after a delay. For LPCS, suppression pool water is simply injected into the RPV above the core due to limitations in the TRACE sparger model. In Limerick, part of the HPCI flow is injected like a core spray; however, in the current TRACE model, all HPCI flow was injected into the feedwater line instead. In Limerick, the LPCI is injected into the core shroud above the core; the current TRACE model has the LPCI injected into the recirculation line like a typical BWR/4 instead, and this will be updated in the future to be consistent with Limerick as well. The LPCI flow rate in the TRACE model is determined based on a pump pressure head calculation, based on the system pressure and other factors, and converted to a pump flow rate using a pump curve. This ensures that the LPCI flow is zero when the system pressure is too high, and the flow becomes positive when the system pressure is low enough.

Net positive suction head (NPSH) calculations were performed for all ECCS pumps to assess cavitation risks, though no cavitation was predicted in any of the LOCA scenarios. Other safety components in the

TRACE model include the reactor protection system (RPS), main steam isolation valves (MSIVs), safety relief valves (SRVs), and turbine bypass valves.

Although the turbine, condenser, and feedwater systems aren't explicitly modeled, control systems simulate their behavior during steady state and transients. During normal (steady state) operation, the feedwater flow rate is managed by a multi-element control scheme based on water level and steam–feedwater flow mismatch, while the feedwater temperature remains constant. Meanwhile, the recirculation flow rate and main steam line pressure are adjusted to achieve the desired mass flow and vessel pressure using TRACE's Constrained Steady State (CSS) feature, which efficiently reaches setpoint values. Reactor power is maintained at its set value during steady state.

During a LOCA transient, the CSS function is disabled, and time-dependent core power values are prescribed. The FW pumps are assumed to trip at 0 sec due to LOOP, causing the FW flow rate to coast down to zero over the first several seconds of the event. The recirculation pump impeller speed is computed using an equation-based method that accounts for inertia. Loss of electric power, consistent with LOOP conditions, causes both pumps to coast down rapidly. The break is modeled as a double-ended (double guillotine) rupture on the suction side of one recirculation loop, with the break area opening linearly to full size within 0.1 s; the break, exposed to slightly above atmospheric pressure, dumps coolant into the drywell.

A limiting single failure in the ECCS is assumed for LWR LOCA analyses. In this work, various failure scenarios were simulated by disabling or reducing the capacity of the relevant ECCS components in the TRACE control models, which altered their transient behavior. Although the TRACE model realistically simulates LOCA for the BWR/4 plant, it is intended solely for this research utilizing a realistic core model and does not intend to meet regulatory requirements or establish a new licensing basis. This research is performed solely to better understand the FFRD phenomena during a postulated LBLOCA. The limiting single failure for the LBLOCA event was assumed to result in the following available systems: 3 LPCI, 1 CS, ADS, HPCI. As stated above, an alternative failure (battery failure) will be investigated in the future as a potentially more limiting failure for Limerick. A double-guillotine break of the RCP suction side was assumed for the LBLOCA event.

As stated previously, the TRACE 3D cylindrical vessel component is divided into two azimuthal sectors and three radial rings. The central two rings represent the volume occupied by the core and inlet/outlet plena. Figure 5 depicts how the TRACE CHAN components correspond to physical bundle locations in the core. All 191 assemblies in the bottom right quadrant are modeled explicitly with a dedicated TRACE CHAN component. Each CHAN component includes a single fluid channel and multiple fuel rod groups: one for each of the BISON rods of interest, and one for the remaining fuel rods in the assembly. Each of these solved fuel rod groups connects to the same common fluid channel, but quench fronts are tracked separately on each of the fuel rod groups. A unique axial power shape and average rod peaking factor was applied to each fuel rod group based on extracting these from the VERA simulation at the end-of-rated cycle exposure statepoint. The Python scripts, discussed below, axially interpolated the VERA axial power values onto the TRACE axial mesh for each fuel rod group. For fuel rod groups containing multiple physical fuel rods, the individual rod axial powers from VERA were averaged over all physical fuel rods in that fuel rod group.

The remaining three quadrants are modeled using lumped channels because the core loading is radially symmetric and previous results have shown that the difference in peak cladding temperature (PCT) results in each of the two azimuthal vessel sectors is negligible during a LBLOCA. Four grouped channels are used to model the majority of the 764 bundles. Each grouped channel is modeled with a single CHAN component in TRACE, the solution of which represents the average TH conditions among all physical bundles in that grouped channel.

There are two grouped channels in each azimuthal sector. These two channels correspond to the inlet orifice map for the Limerick plant and each also corresponds to a radial ring in the TRACE vessel component. Grouping the channels in this manner allows the inlet orifice K-factors to be assigned appropriately to the bundles. It also ensures that the bundles in the outer ring of the core do not artificially reduce the PCT values and other results within the central channel; the outer ring consists of twice-burned bundles, and their power level and fuel/cladding temperatures are much lower than bundles in the core interior. The average power and burnup conditions for these grouped channels are given in Table 2.

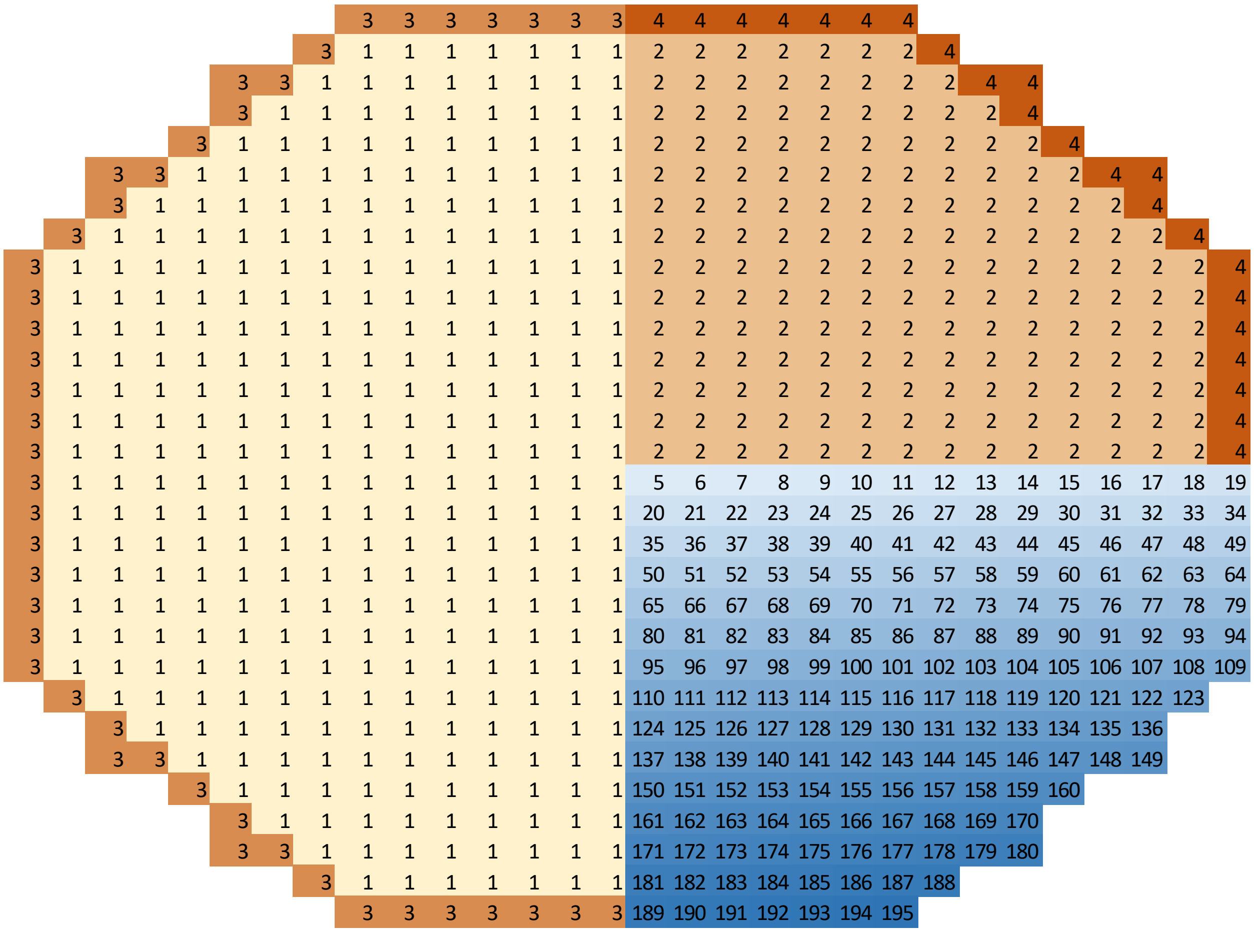

Figure 5. TRACE channel configuration.

Table 2. Bundle-Averaged Power and Burnup Conditions in the TRACE Lumped Channels, at EOC in the Cycle of Interest

TRACE Channel Number	**Description**	**Assembly Power Factor**	**Assem Exposure [GWd/MTU]**
1	**Average core (Ring 1, Az. 1)**	1.109	36.173
2	**Average core (Ring 1, Az. 2)**	1.109	36.173
3	**Average core (Ring 2, Az. 1)**	0.192	49.077
4	**Average core (Ring 2, Az. 2)**	0.192	49.077

945 individual rods were modeled among the 191 assemblies, with axial powers and burnups taken from VERA and with TRACE results passed to BISON for transient analysis. Core boundary conditions and core power/burnup distributions were based on the Limerick third cycle of interest at the end-of-rated-power burnup statepoint.

A series of Python scripts was developed to streamline modifications to the TRACE input file for these analyses. The process for generating the TRACE input file proceeds as follows:

1. First, a base TRACE input file is produced using the SNAP graphical user interface. This file fully implements models for the RPV, BOP, control systems, and safety systems during both steady state and transient conditions—but it initially contains only one representative core channel with uniform power and burnup conditions as placeholders.
2. Next, the Python scripts parse the complete text-based TRACE input file into its main sections (such as Namelist Data and Component Data) and further divide these into individual system components. Each component's data—whether scalar, array, or string—are stored in Python dictionaries to enable easy manipulation.
3. The single channel component from the base input is then duplicated into the desired number of channel components. Each duplicate is connected to the specified vessel cells and customized to represent the correct number of physical channels (bundles) along with additional channel-specific data. This process uses Python routines to copy the existing dictionaries, modify entries, attach the component to the vessel and power models, and update other portions of the input file. The channel definitions are provided through a JSON file.
4. In a separate step, another Python script extracts axial rod power and burnup values from a VERA HDF5 data file. These values are first averaged for each bundle and then averaged across all bundles within each TRACE grouped channel, according to a 2D channel map. The resulting axially dependent, channel-averaged values are interpolated onto the TRACE axial mesh and populated into the corresponding Python dictionaries for each channel.
5. Finally, the modified set of data dictionaries is written out to a new TRACE input file that reflects all the changes made to the model.

This script-based approach avoids the need for repetitive, manual modifications—which are both time-consuming and prone to error—in large models. Such a task would be intractable to manage in SNAP by manually copying and modifying each channel for all 195 channels in the current TRACE model. Additionally, any changes to the base channel input (such as updates to fuel rod modeling, geometric parameters, or T/H settings) are automatically applied to all channels in the final model, eliminating the need to edit each channel component individually every time a modification is made.

The scripting functionality is rigorously validated through a suite of unit tests to ensure that modifications to the TRACE input file are accurate. These tests include:

- Parsing the entire TRACE input file into a Python dictionary format, then writing it back to a text file and verifying that the output matches the original file perfectly.
- Applying various modifications to the TRACE data—such as duplicating components and assigning power values—and comparing the results to input files that were manually generated in SNAP. This ensures that the automated modifications are correctly implemented.

This testing framework provides confidence in the reliability and correctness of the scripting approach.

4.3 LARGE-BREAK LOCA RESULTS

The LBLOCA event progression and timings predicted by TRACE are given in Table 3. The break, scram initiation, MSIV closure initiation, and recirculation pump trips are all assumed to occur within the first 1.0 s of the event. HPCI and RCIC injections begin at 32.3 s based on detection of a low RPV water level with an assumed actuation delay time. LPCS injection begins at 46.9 s and LPCI injection follows soon afterward at 53.0 s.

Table 3. LBLOCA Event Progression and Timings as Predicted by TRACE

Simulation Time (s)	Event
0.0	Break occurs (0.1 s duration)
0.0	Scram initiates
0.0	FW pumps trip
0.5	MSIV closure begins (3.0 s duration)
1.0	Both recirculation pumps trip
32.3	HPCI injection begins
46.9	LPCS injection begins
53.0	LPCI injection begins
112.6	Max outer surface PCT occurs

Rod PCT results for the large break LOCA case are shown in Figure 6. Note that these PCT results refer to the outer surface of the rod. In reality, the true PCT will be on the interior of the rod, but during the reduced power conditions of LBLOCA, the inside and outside surface temperatures will be close in value. Rod temperatures decreased for approximately the first 20 s of the event due to decreased post-scram power and due to the cooling effects of blowdown. Once the core was sufficiently uncovered, fuel and cladding temperatures began to rise in a fairly linear manner. This was due to the continued generation of decay power within the rods which exceeded the steam cooling capability in the core.

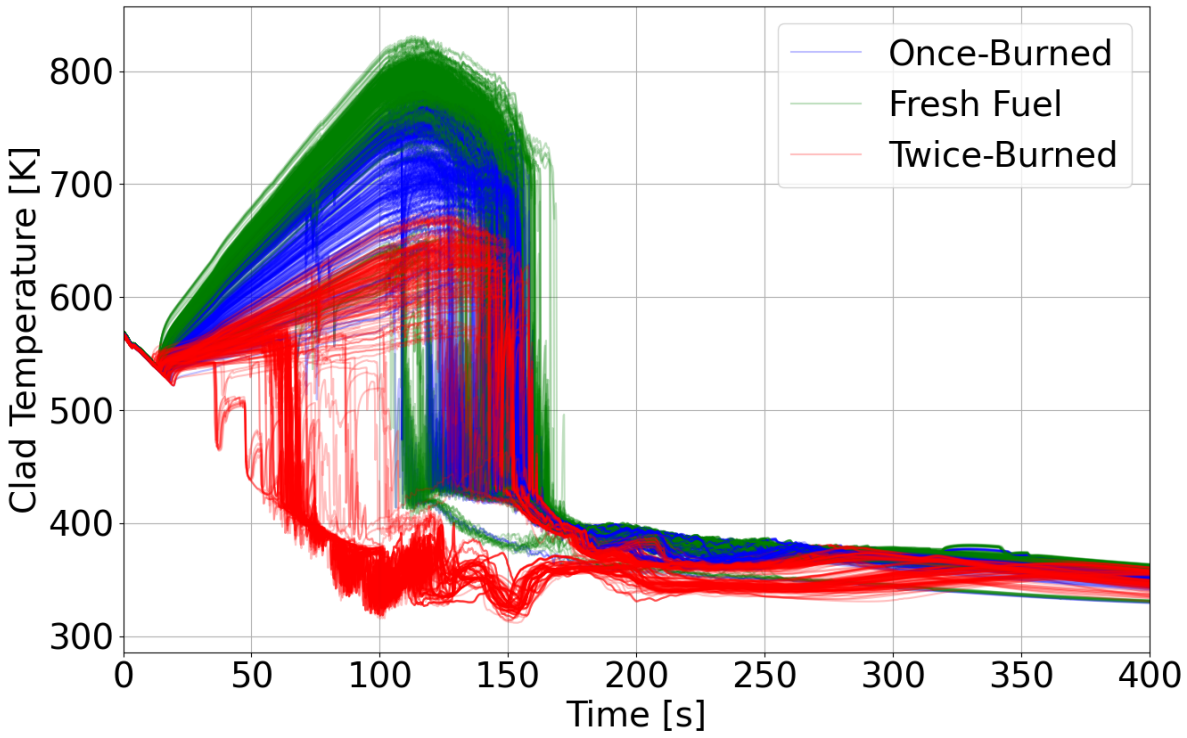

Figure 6. Rod outside surface PCT versus time for each of the rods of interest.

Figure 7 shows the cladding heatup rate for each of the rods. The simplest way to calculate the cladding heatup rate would be to take the slope of the cladding temperatures from one timestep to the next. However, this is highly prone to the effects of numerical fluctuations in the cladding temperature data, resulting in unrealistically extreme cladding heatup rate values at many of the timesteps.

A more realistic method is to apply an averaging process over a series of consecutive timesteps. The cladding heatup rate is calculated by first computing the time derivative (dT/dt) of the cladding temperature at each axial location using finite differences between consecutive time points. To reduce numerical noise from the finite difference calculation, a moving average filter with a window size of 50 points is applied to the raw heatup rate time series using a uniform kernel via Python numpy's convolution function. This time window corresponds to approximately 10 s of transient time, since the plotting interval of the TRACE data is typically 0.2 s. The smoothed heatup rates are then evaluated across all axial locations and time points to determine the maximum value. For time series plotting, the smoothed heatup rate at the specific axial location where the outside surface PCT occurs is stored and used to generate consistent, noise-reduced results.

After the initial temperature drop over the first 20 s of the event, cladding heatup rates rise to as high as 6 K/s in the highest power fresh rods, then more or less stabilize at a lower value during the decay energy heatup phase of the event. Cladding heatup rates during this time range from near 0 K/s to 3 K/s depending primarily on the rod power factor. Once a given rod quenches, a negative "heatup" rate is produced. One of the once-burned rods exhibited a large negative clad heatup rate at approximately 110 sec followed by a large positive heatup rate at approximately 120 sec. This occurred because TRACE predicted a nearly-instantaneous quench of the rod followed by re-dryout, causing a rapid dip then rebound in temperature. This behavior was observed to a lesser extent in some other rods as well. However, due to its infrequent and sporadic nature, and the fact that this is not consistent with the more

gradual dryout and rewetting behavior expected from the quench front propagation processes, it was concluded that this behavior was numerical in nature and an artifact of the TRACE timestepping numerical convergence process. It is not considered to be a physically realistic result.

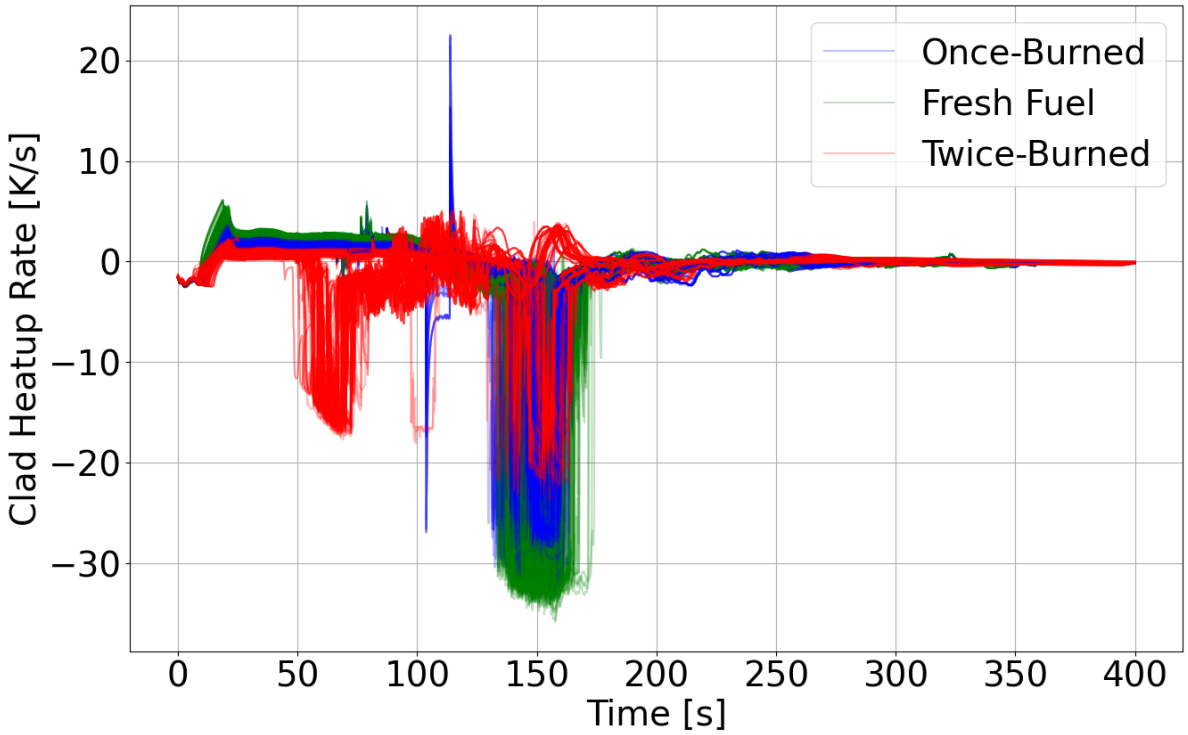

Figure 7. Cladding outside surface heatup rate versus time for each of the rods of interest.

The first ECCS injections were assumed to begin at 32 s, with each ECCS component beginning and terminating injection based on appropriate setpoints and delay times. The flow rates versus time of the ECCS components are shown in Figure 8. The HPCI and RCIC were assumed to inject into the feedwater line, the LPCI was assumed to inject into the recirculation loops, and the core spray was assumed to inject into the vessel volume directly above the core.

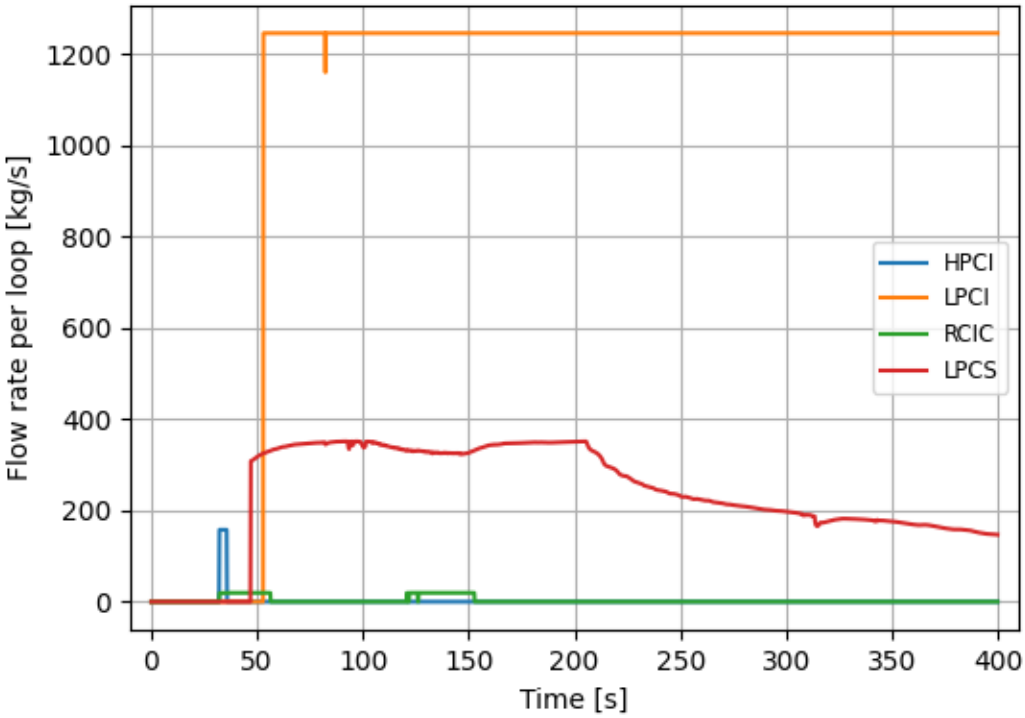

Figure 8. ECCS coolant flow rates versus time during the large break LOCA event.

Once sufficient ECCS coolant had been injected into the vessel and core, the liquid water level began to rise up the length of the fuel rods, cooling the rods along the way. The highest-PCT rod in the core was one of the rods in Assembly 96, and the quench front elevation versus time for this rod is shown in Figure 9. TRACE calculates two separate quench fronts: one beginning at the bottom of the core and moving upward due to the increasing liquid water level of the core (reflooding), and one beginning at the top of the core and moving downward due to liquid injection from the core spray system above the core. The PCT typically occurs at the upper part of the fuel rod where power peaking factors are high and where the quench front takes longer to arrive. The hot spot in all rods quenched prior to 175 s, and many rods quenched considerably earlier. This was especially true for low-power, twice-burned rods which more readily quenched due to low cladding temperatures and low rate of vaporization in the coolant.

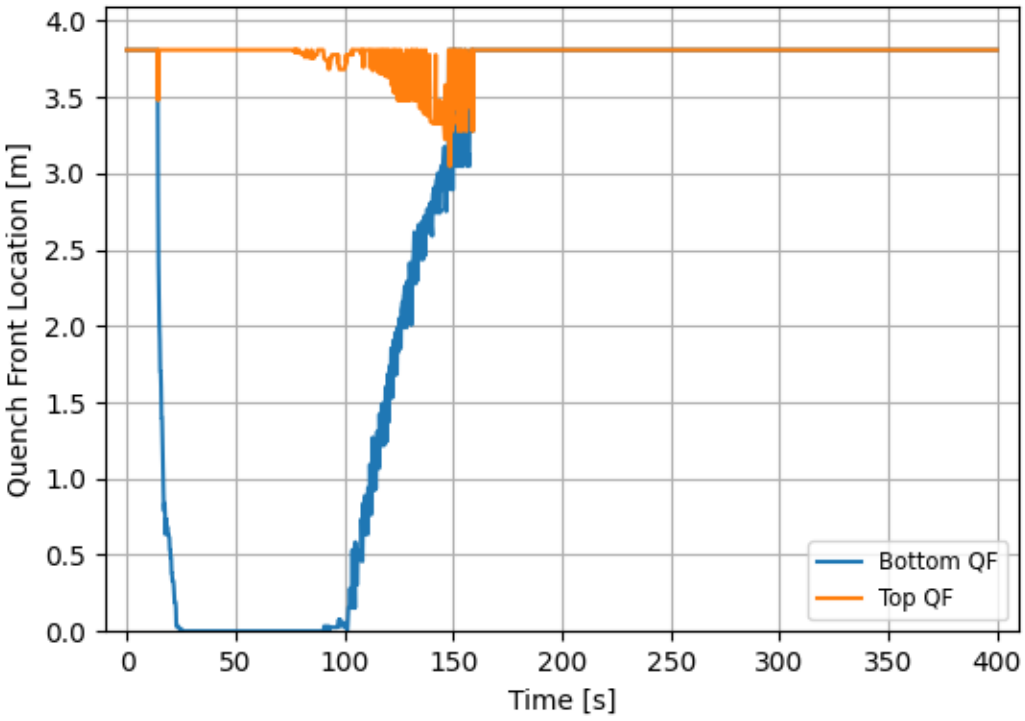

Figure 9. Quench front elevation for the highest outside surface PCT rod in the core.

Figure 10 shows the relationship between a rod's maximum outside surface PCT during the event and the rod's average power and burnup levels. Figure 11 shows a similar comparison for the local power and burnup levels at the elevation where the maximum outside surface PCT occurred. A clear trend is seen in terms of the maximum outside surface PCT and power, with the maximum outside surface PCT increasing relatively linearly with both the rod-average and local power value. Note that a number of twice-burned fuel rods during the LOCA never exceeded or barely exceeded the steady state cladding temperature (roughly 570 K), resulting in a separate cluster of datapoints at roughly the 570 K level.

The trend between the maximum outside surface PCT and burnup appears to be largely indirect; higher-burnup rods tend to have lower power, which in turn leads to lower outside surface PCT values. Based on the high scatter in the datapoints of the burnup plots, there appears to be little direct effect of burnup on the maximum outside surface PCT. Burnup impacts the steady state pellet temperature distribution, and therefore the initial stored energy in the fuel rods, by impacting the gap size and burnup-dependent fuel conductivity. However, this initial stored energy in the BWR fuel does not cause cladding temperature to rise in the first few seconds of the event, as was predicted previously for PWRs. The cladding temperature instead drops throughout the blowdown phase. This is true for all rods included in this study, across the full range of power and burnup conditions indicated in Figure 10 and Figure 11. The reason for this is likely the lower power density in the BWR, lower stored energy of the fuel, and relatively more inventory in BWR vessels (compared to PWRs). Furthermore, nucleate boiling and steam cooling play a significant role in the BWR LOCA response and are effective at removing the stored heat from the fuel rods during the initial blowdown phase of the event. This causes the cladding temperatures to be very close to the

saturated temperature during this time. After the blowdown phase, the temperature rise across the pellet is small due to the low linear heat rate associated with decay power, so any impact of higher burnup on the cladding temperature is likely insignificant. Therefore, the local or rod-average power level is the primary driver of outside surface PCT during the event. It is worth noting that the location of the high-burnup pin is also important, as placement in a region near fresh fuel that has higher power will lead to higher temperature in the high-burnup pin.

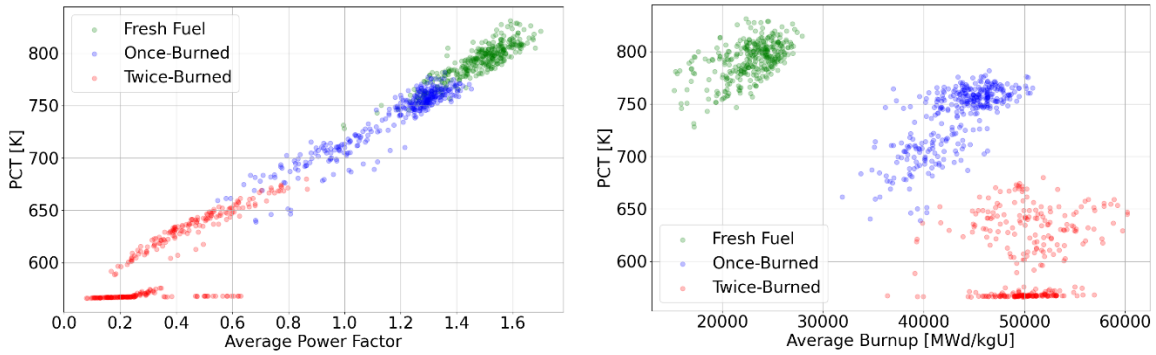

Figure 10. Maximum rod outside surface PCT for the rods of interest during the LOCA event, plotted against the average power factor and burnup of the rod.

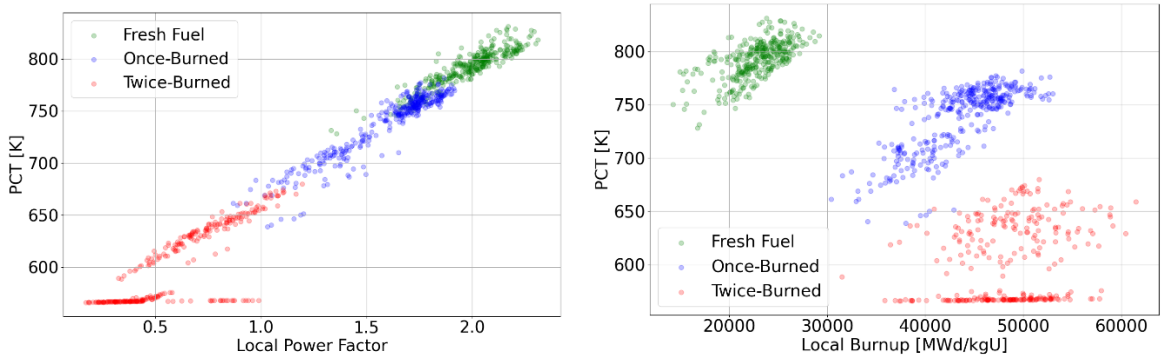

Figure 11. Maximum rod outside surface PCT for the rods of interest during the LOCA event, plotted against the local power factor and burnup at the PCT location.

4.4 SMALL-BREAK LOCA RESULTS

A representative SBLOCA analysis was performed to estimate the fuel and cladding response for several break sizes. This analysis is more conservative than the plant response due to LPCI being directed into suppression pool cooling (instead of to the vessel) as discussed below; therefore, these results should be considered preliminary and future work will be needed to model the SBLOCA response more realistically. A more detailed break spectrum analysis, with more small and large break sizes analyzed, will also be needed.

The impact of break size was investigated by adjusting the flow area exiting the suction side of the broken recirculation loop. For reference, the flow area of the recirculation line is 3620 cm^2, and the LBLOCA analysis assumed a double guillotine break, therefore this 3620 cm^2 break size was applied to both sides of the broken pipe during the LBLOCA event. The small-break LOCA (SBLOCA) analysis in this section assumed the recirculation line remained intact and only a single opening of the stated break size was

modeled. An initial scoping study was performed to determine the approximate magnitude of break sizes that result in SRV cycling while maintaining a quasi-stationary pressure level for several minutes prior to ADS actuation. Such behavior is typical of limiting SBLOCA analyses in plants of this type. Break sizes of 36 cm^2 and above caused depressurization that was too fast to allow pressure stabilization through SRV cycling, resulting in rapid actuation of the ADS and no increase in outside surface PCT. The expected SRV cycling behavior was seen at smaller break sizes, including some increase in outside surface PCT. For that reason, break sizes of 3.6 cm^2, 9.1 cm^2, and 18.1 cm^2 are shown in this section.

HPCI and RCIC were assumed to be unavailable during the SBLOCA (single failure assumption). The available ECCS components were 4 LPCI, 2 CS, and ADS. As with LBLOCA, the case of battery failure will be investigated as a potentially more limiting single failure in future work.

The timing of key events during the SBLOCA as predicted by TRACE for the 9.1 cm^2 break case is shown in Table 4. ECCS flow rates over time are shown in Figure 12. There appears to be an issue with how the LPCI control system was configured in the current TRACE model, which led to zero LPCI flow into the primary loop for the duration of the event. Upon further investigation, the control system for the RHR system caused the RHR to be actuated at 712.0 s, but the flow was discharged to the suppression pool in suppression pool cooling mode. Typically, the RHR flow during a SBLOCA event should inject into the primary system in LPCI injection mode instead. This modeling lineup results in more conservative SBLOCA results in this analysis due to less ECCS availability. Note that this issue did not occur during the LBLOCA analysis, for which the LPCI flow was delivered to the primary system as expected. This issue impacted only the current SBLOCA analyses. LPCS flow did successfully inject into the vessel, but LPCI would increase the total cooling available during the SBLOCA event. Future work could address this issue, as it has the potential to alter the event progression, limiting break size, and maximum outside surface PCT.

Table 4. SBLOCA Event Progression and Timings as Predicted by TRACE

Simulation Time (s)	Event
0.0	Break occurs (0.1 s duration)
0.0	Scram initiates (LOOP assumption)
0.0	FW pumps trip
0.6	MSIV closure begins coincident with LOOP (3.0 s duration)
1.1	Both recirculation pumps trip (LOOP assumption)
60.8	SRV cycling begins
571.5	ADS actuates
704.2	LPCS injection begins
712.0	Suppression pool injection begins
730.0	Maximum outside surface PCT occurs

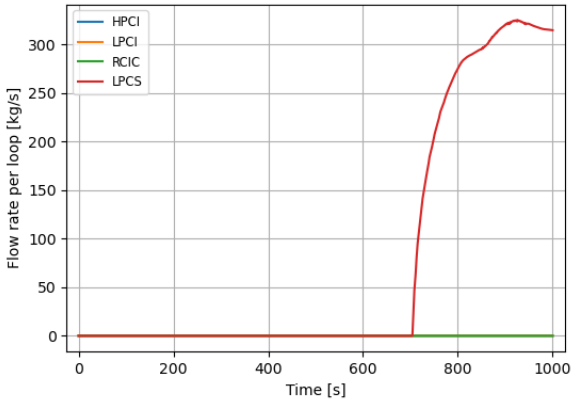

Figure 12. ECCS flow rates during the SBLOCA event.

Results are shown in Figure 13 through Figure 18 for the three break sizes. The current TRACE results demonstrated the expected behavior of SRV cycling until 571.5 s when the ADS actuates. At this point, SBLOCA analyses typically observe an increase in cladding temperature due to uncovery of the upper region of the core after flashing of the core inventory as the pressure reduces. TRACE intermittently predicts uncovery of the upper portion of the fuel starting around 750 s in the 3.6 cm^2 break case, 500 s in the 9.1 cm^2 break case, and 320 s in the 18.1 cm^2 break case. In these latter two cases, fuel uncovery and outside surface PCT rise actually began prior to ADS actuation. Prolonged heatup lasting roughly 200 s occurred in the 18.1 cm^2 break case, but the other two cases in particular exhibited briefer intervals of rapid heatup followed quickly by rewet.

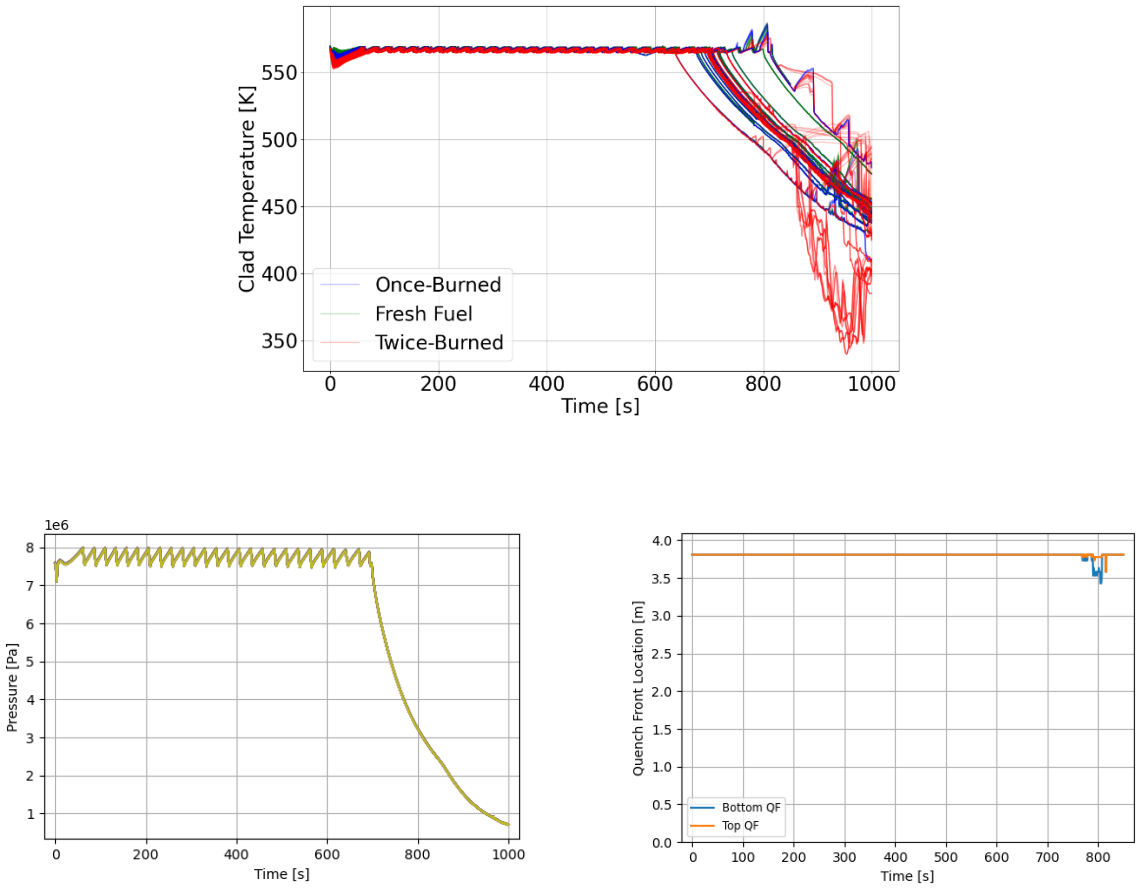

Figure 13. Outside surface PCT (top), primary loop pressure (bottom left), and hot rod quench front elevation (bottom right) during a SBLOCA with a break size of 3.6 cm^2.

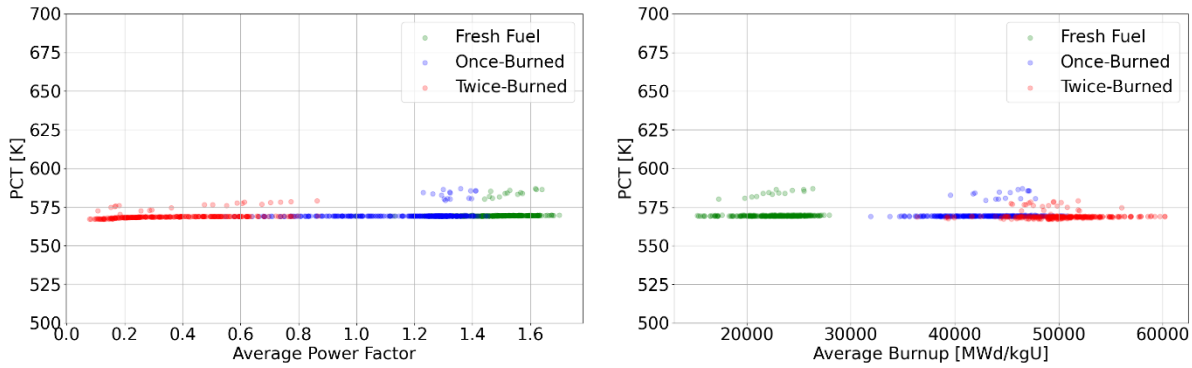

Figure 14. Maximum rod outside surface PCT for the rods of interest during the SBLOCA event with a break size of 3.6 cm^2, plotted against the average power factor and burnup of the rod.

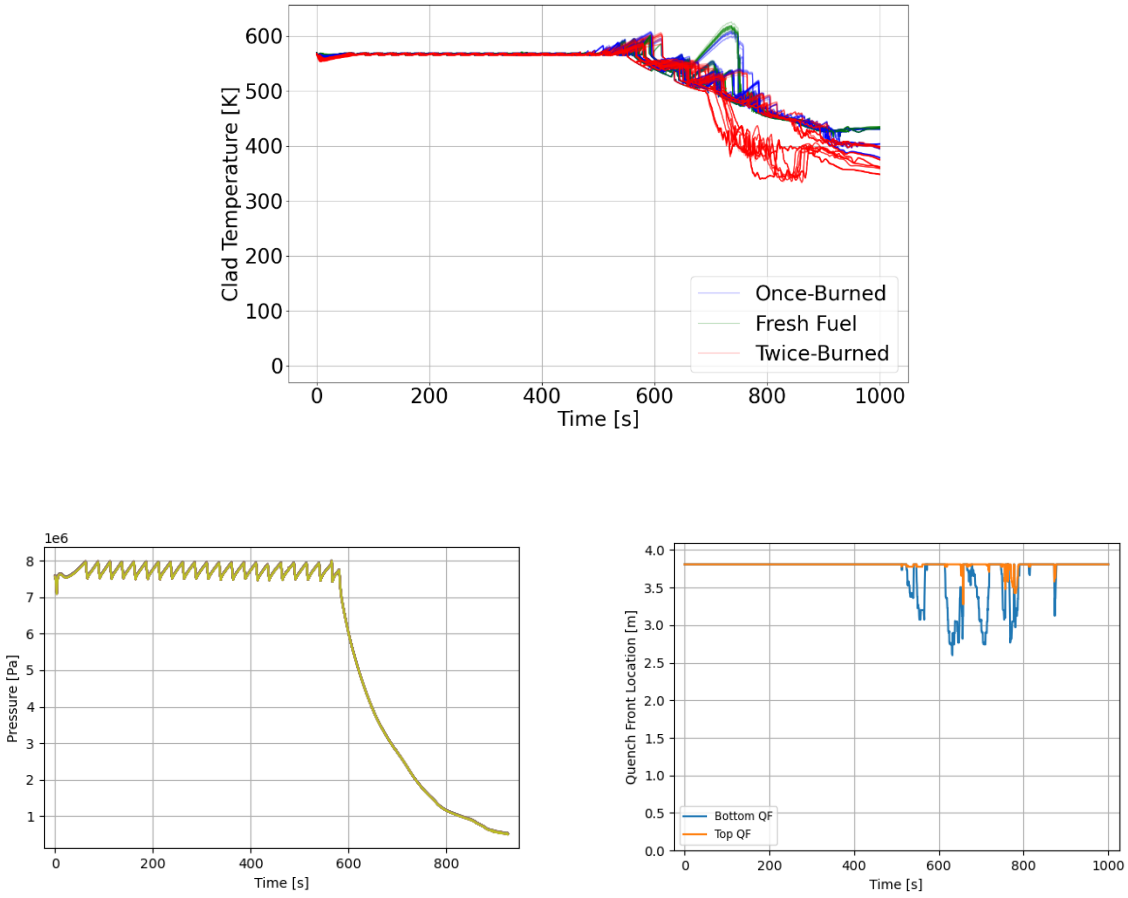

Figure 15. Outside surface PCT (top), primary loop pressure (bottom left), and hot rod quench front elevation (bottom right) during a SBLOCA with a break size of 9.1 cm^2.

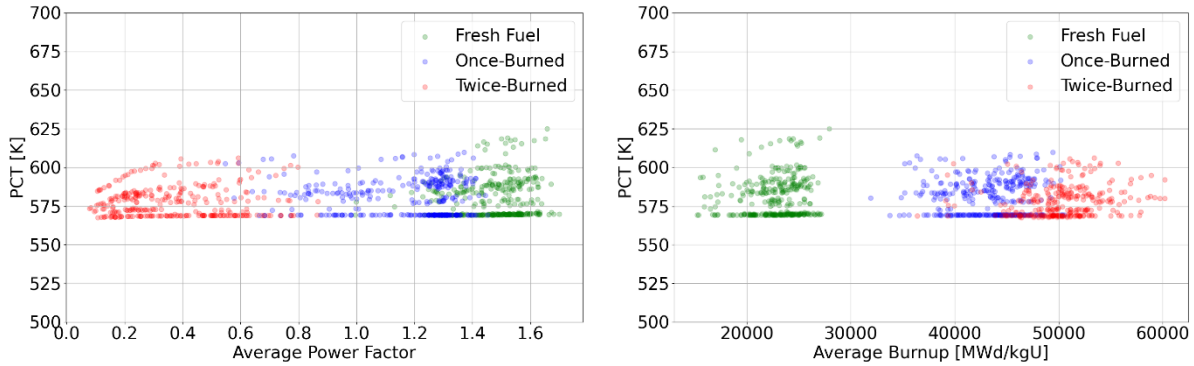

Figure 16. Maximum rod outside surface PCT for the rods of interest during the SBLOCA event with a break size of 9.1 cm^2, plotted against the average power factor and burnup of the rod.

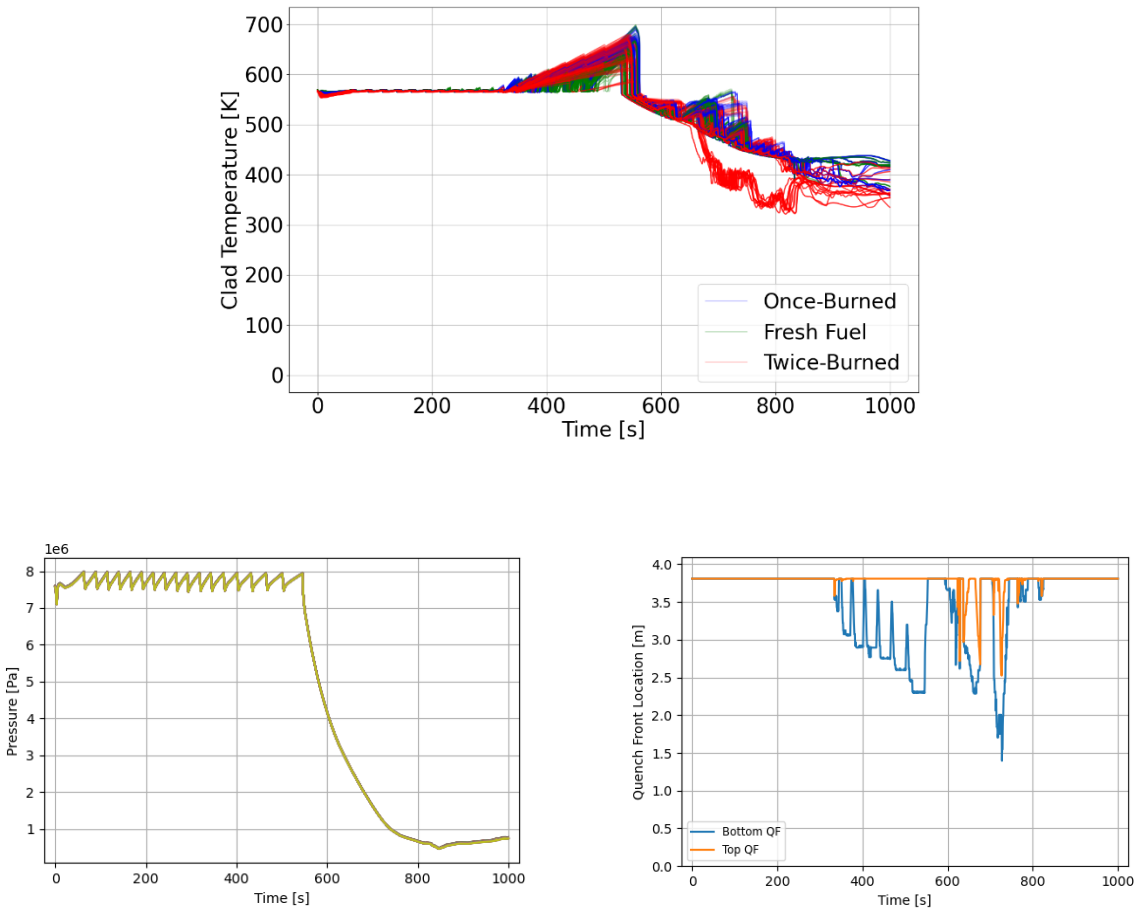

Figure 17. Outside surface PCT (top), primary loop pressure (bottom left), and hot rod quench front elevation (bottom right) during a SBLOCA with a break size of 18.1 cm^2.

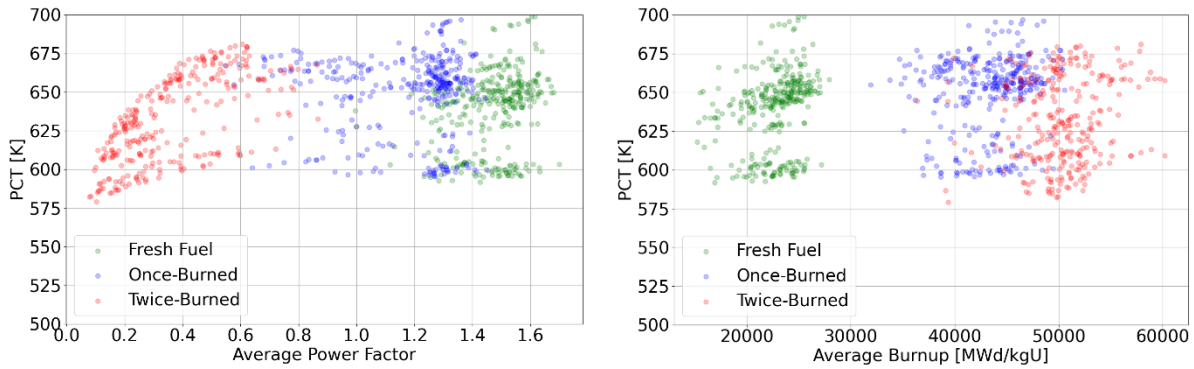

Figure 18. Maximum rod outside surface PCT for the rods of interest during the SBLOCA event with a break size of 18.1 cm^2, plotted against the average power factor and burnup of the rod.

5. BISON TRANSIENT ANALYSIS

5.1 SIMULATION SETUP

BISON was used to predict the fuel and cladding performance of the 945 rods simulated individually in TRACE. A custom Python script was used to transfer TRACE results—cladding surface temperature, rod average power, axial peaking factors, and coolant pressure—to the BISON input files as boundary conditions. In addition, two cladding burst models were added to the input files. The Chapman correlation (CC) is an empirical correlation that calculates a burst temperature from the cladding hoop stress and heating rate. If the local cladding temperature exceeds the burst temperature, then the correlation predicts cladding burst [11,12]. The strain-rate criterion (SRC) is a much simpler correlation. It predicts cladding burst if the strain rate exceeds 100 h^{-1} [13]. Most other edits to the BISON input files were done to facilitate these two models. Both the CC and SRC have been used to predict cladding burst in previous works [2,5].

In BISON, cladding burst is modeled as a Boolean variable. A value of 0 indicates cladding that is intact, whereas a value of 1 indicates that a burst has occurred at that location. This is a simple approach to analysis, but it means that after burst has occurred, many of the predictions are no longer reasonable because they do not capture behaviors like plenum gas venting, plenum flooding, or fuel dispersal. Therefore, the simulations were set to terminate if both models had predicted burst.

5.2 SIMULATION RESULTS

All 945 simulations ran to completion. One rod exceeded the current 62 GWd/MTU burnup limit. Neither the CC nor the SRC showed any cladding ruptures during normal operation or during the LOCA. The normal operation results are shown at the end of cycle (immediately before the LOCA) in Figure 19. There are obvious groupings based on how many cycles the rods have been in the core. The LHR and temperature profiles decrease with burnup. FGR, plenum pressure, and hoop strain increase with burnup. However, FGR, plenum pressure, and hoop strain reach their maximum values among once-burned rods. This is because the most aggressively irradiated rods are removed after two cycles, so they do not appear in the twice-burned group. Note that PCT in subfigure (b) refers to inner surface PCT, which is the case for all BISON results. Also, note that the hoop strain is positive in low-burnup rods due to thermal expansion during reactor operation. Typical post-irradiation measurements would be done on cold rods and find negative strains on low-burnup rods.

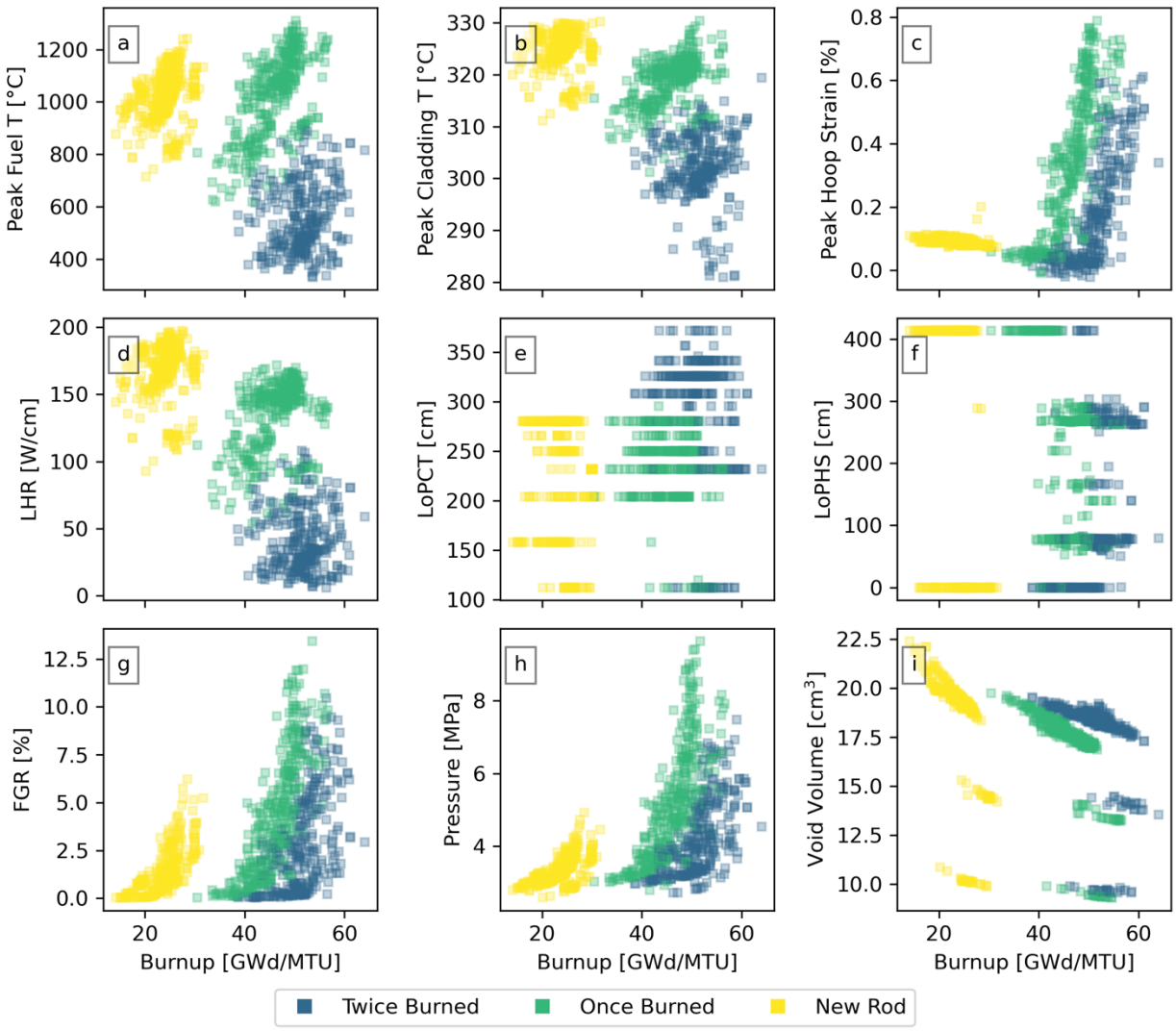

Figure 19. Fuel performance predictions at the end of normal operation during the cycle of interest. Predictions of interest include a) PFT, b) inner surface PCT, c) peak hoop strain, d) LHR, e) location of inner surface PCT, f) location of peak hoop strain, g) FGR, h) plenum pressure, and i) void volume. The x-axes show the burnup of the fuel rods and the colors represent the number of cycles in which the rods have been in the core.

The transient results are shown in Figures 20–26. The same formatting is used in each of these figures. The left side (a) shows the BISON prediction during the complete operating histories (up to three cycles) and the right side (b) shows the same prediction during the LOCA. The color represents the number of cycles in which the rod has been irradiated. Figure 20 shows the LHR, Figure 21 shows the peak fuel temperature, Figure 22 shows the peak cladding temperature, Figure 23 shows the plenum pressure, Figure 24 shows the void volumes, Figure 25 shows the peak cladding hoop strain, and Figure 26 shows the peak cladding hoop stress.

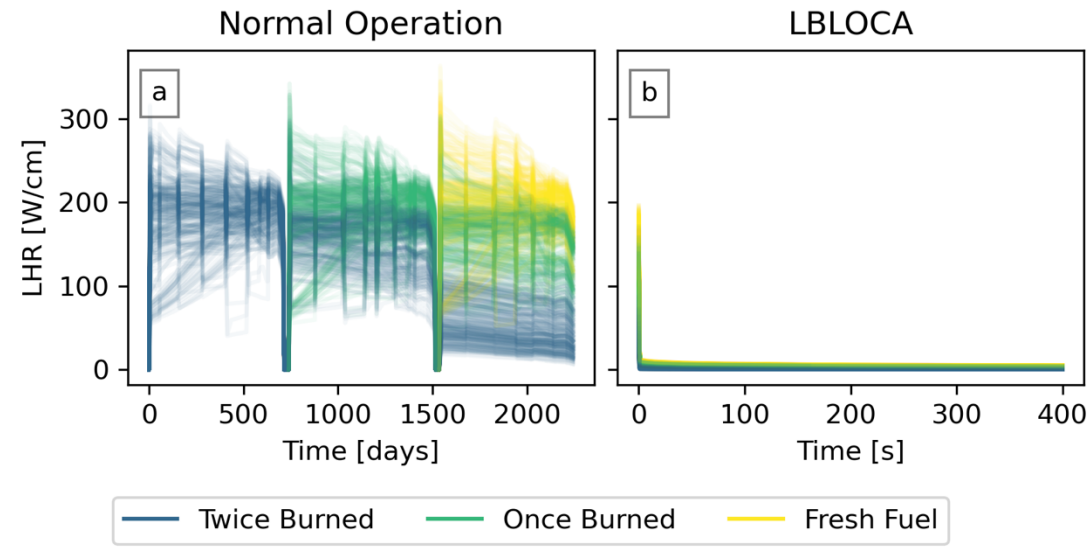

Figure 20. BISON LHR predictions during a) normal operation, and b) the LOCA. Colors represent the number of cycles in which the rods have been in the core.

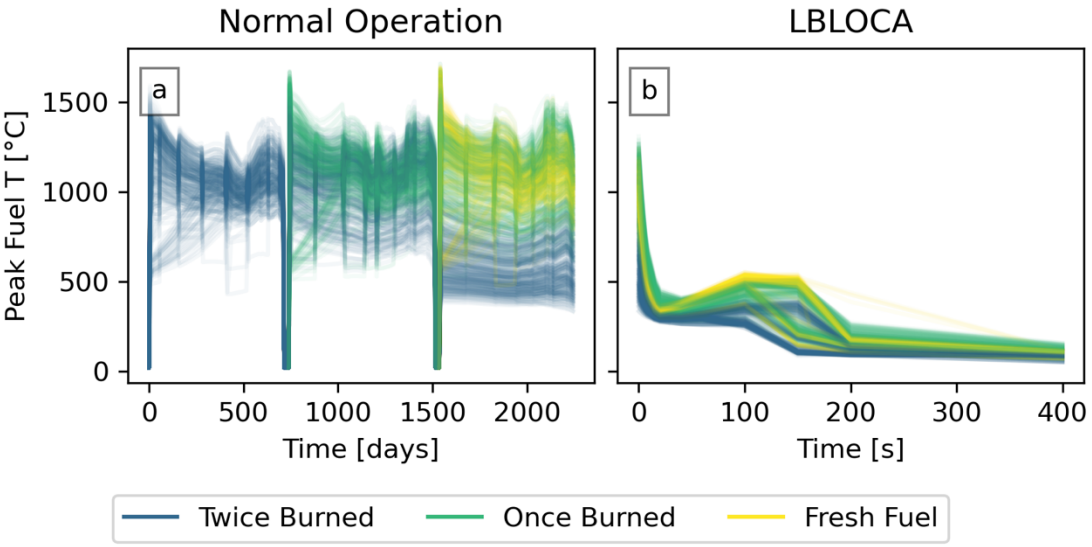

Figure 21. BISON PFT predictions during a) normal operation and b) the LOCA. Colors represent the number of cycles in which the rods have been in the core.

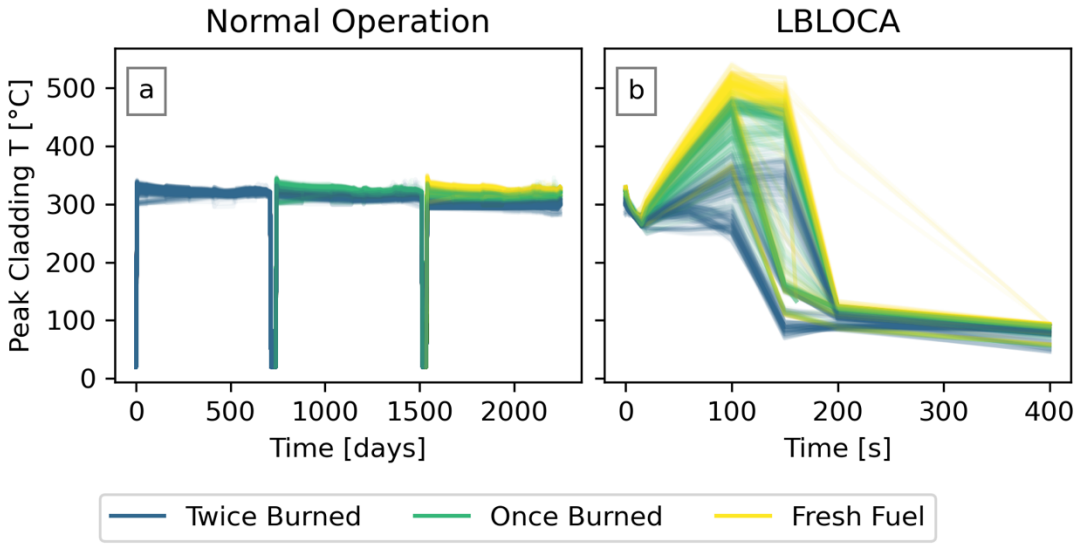

Figure 22. BISON inner surface PCT predictions during a) normal operation and b) the LOCA. Colors represent the number of cycles in which the rod has been in the core.

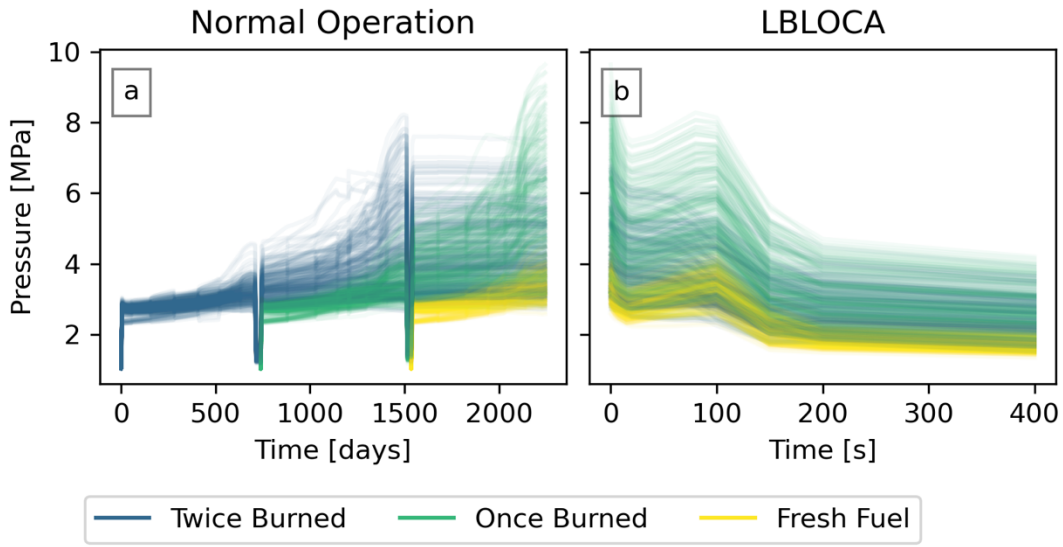

Figure 23. BISON plenum pressure predictions during a) normal operation, and b) the LOCA. Colors represent the number of cycles in which the rod has been in the core.

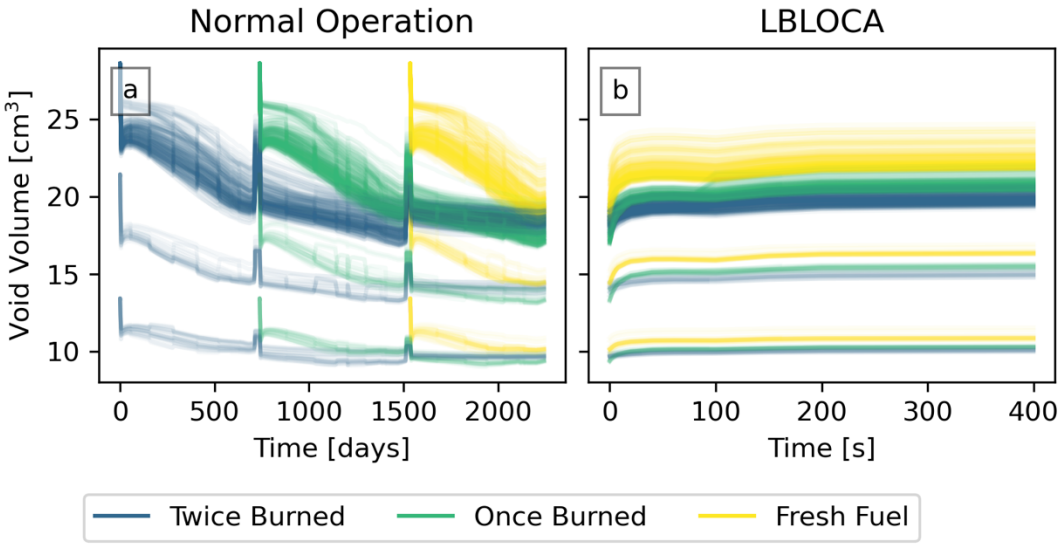

Figure 24. BISON void volume predictions during a) normal operation, and b) the LOCA. Colors represent the number of cycles in which the rod has been in the core.

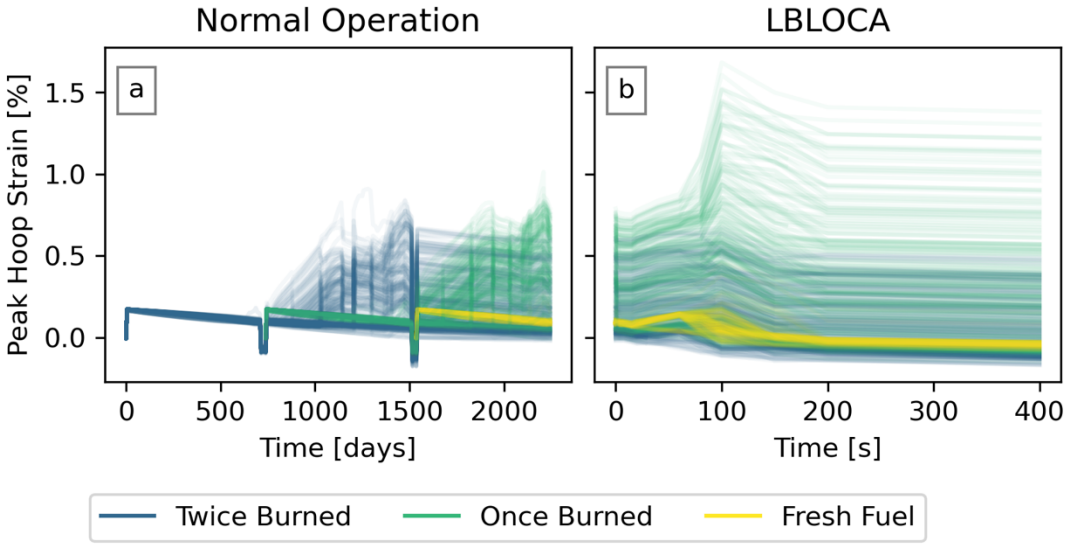

Figure 25. BISON peak hoop strain predictions during a) normal operation, and b) the LOCA. Colors represent the number of cycles in which the rod has been in the core.

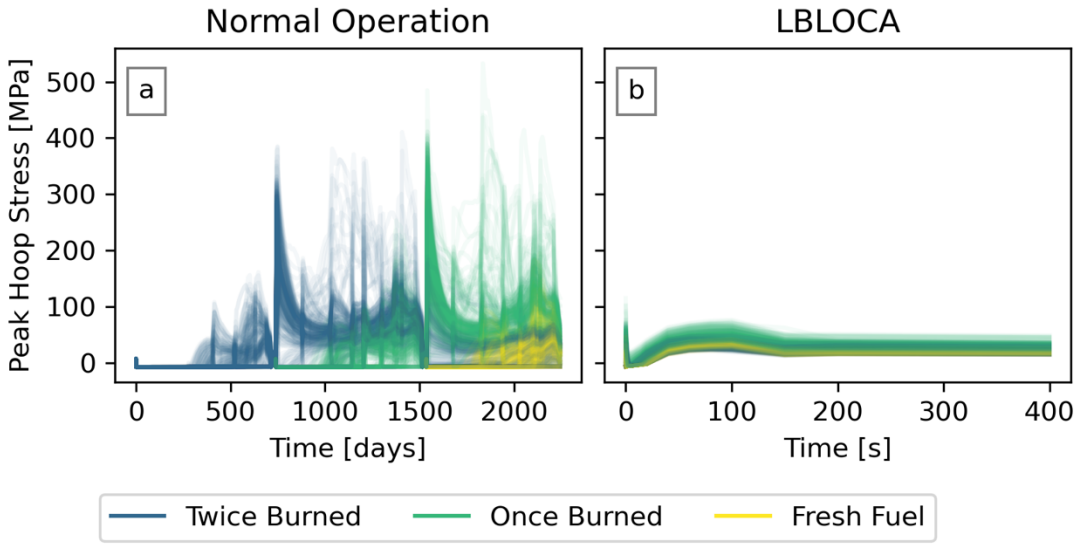

Figure 26. BISON peak hoop stress predictions during a) normal operation and b) the LOCA. Colors represent the number of cycles in which the rods were irradiated.

The LHR is one of the boundary conditions imported from TRACE. The results show the scram happens immediately and all rods drop to zero power regardless of their pre-transient power. During normal operation, the fuel and cladding temperatures are stratified according to the number of cycles the fuel has been in the core. However, during the transient, the fuel and cladding temperature equalize. The fuel temperature drops as the cladding temperature rises.

During normal operation, the plenum pressure increases with burnup in an exponential profile. However, the exponential rate varies significantly between rods as complex thermal, mechanical, and irradiation feedback effects control the rate of FGR. During the transient, the plenum pressure initially is relatively unchanged but begins dropping at about 100 s as the temperatures drop.

During the LOCA, the hoop stress drops and then rebounds, but never reaches the same magnitude as during normal operation. The stress drops in the cladding because pellet-clad contact is no longer contributing to the stress. Additionally, the fuel contracts and the plenum temperature decreases as it cools, reducing pressure on the cladding and reducing stress. As the cladding heats up, it begins to thermally expand with only negligible effects on stress. However, the coolant pressure decreases during the LOCA, causing a significant pressure differential that increases the cladding strain. This increase in the strain is what allows the plenum pressure to begin falling at the 100 s mark.

The peak hoop stress is abnormally high during normal operation and warrants further investigation. Figure 27 shows the location at which the stress occurs, and the mechanism becomes apparent. The stress is caused by the fuel's axial expansion forcing a sudden radial strain on the cladding. This behavior is facilitated by the frictionless contact assumption used in these simulations. Therefore, future simulations should begin to use frictional contact to reduce this erroneous stress.

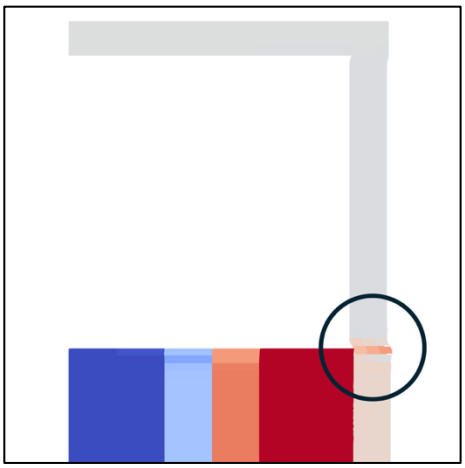

Figure 27. Top section of a fuel rod with a high peak hoop stress in the cladding. The image has been expanded by a factor of 30 in the radial direction. The location of the peak hoop stress is circled.

5.3 DISCUSSION

The cladding burst predictions for the two models considered are summarized in Table 5. For comparison, the same models from a previous study in PWRs predicted all—or all except one depending on the cladding burst model—once-burned rods would burst. These predictions do not prove that BWRs are less susceptible to FFRD than PWRs. Such a conclusion would assume there are no reactor-specific factors that contribute to the conditions leading to burst and therefore FFRD. Considering that the PWR study used a theoretical, aggressive high-burnup core loading pattern, that is not a valid assumption. However, it is likely that Limerick 1's relatively low cladding temperature and rod internal pressure played a role in the FFRD predictions.

Table 5. CC and SRC cladding burst predictions for BWRs

History	Chapman Correlation	Strain Rate Criterion	Total Rods
Fresh Fuel	0	0	335
Once Burned	0	0	330
Twice Burned	0	0	282

6. BISON SENSITIVITY AND UNCERTAINTY ANALYSIS

As stated above, VERA predictions of BWR power profiles have been found to have mid-cycle errors of up to 15%. Therefore, it is worth establishing if these uncertainties can affect the FFRD predictions.

6.1 STUDY SETUP

A custom Python script was used to modify the BISON LOCA input files. A multiplication factor was applied to the average LHR function with values of 1.05, 1.10, and 1.15, to increase the LHR by 5, 10, and 15%, respectively. However, there are feedback effects between LHR and other inputs in the fuel performance simulations. The cladding outer surface temperature was also adjusted to account for a higher heat flux to the coolant. The algorithm to make this adjustment is described below. All 945 rod-specific simulations were re-run with these three factor values, resulting in 2,835 additional simulations.

The previous BISON simulations did not include the coolant. Rather, they imported cladding surface temperatures from VERA or TRACE depending on the point in the simulation. For this analysis, it was assumed that the cladding surface temperature matched the coolant temperature at every axial location. For a function with n axial positions along the cladding, the cladding surface temperature used for the sensitivity study is set to match the original temperature at $z = z_0$, such that

$$T_{s,0} = T_0, \tag{1}$$

where T_0 is the nominal surface temperature at $z = z_0$ and $T_{s,0}$ is the sensitivity surface temperature. Next the inlet enthalpy, h_0 is calculated using the IAPWS equation of state [14],

$$h_0 = IAPWS(P, T_0). \tag{2}$$

The IAPWS formulation always requires two inputs. The coolant pressure, P is always used as one of the inputs in this algorithm. Since the sensitivity surface temperature matches the original surface temperature at z_0, the enthalpies match as well, $h_{s,0} = h_0$.

Next, for each axial position, z_i, on the rod where $i > 0$, the nominal surface temperature is once again used to calculate the enthalpy:

$$h_i = IAPWS(P, T_i), \tag{3}$$

and the change in enthalpy is calculated as

$$\Delta h = h_i - h_{i-1}. \tag{4}$$

The sensitivity temperature can then be calculated using the IAPWS formulation as

$$T_{s,i} = IAPWS(P, h_{s,i-1} + f\,\Delta h), \tag{5}$$

where f is the multiplication factor. The algorithm continues until the boiling temperature is reached, at which point the temperature remains constant for the remainder of the rod. An example of the change in temperature profile caused by this algorithm is shown in Figure 28.

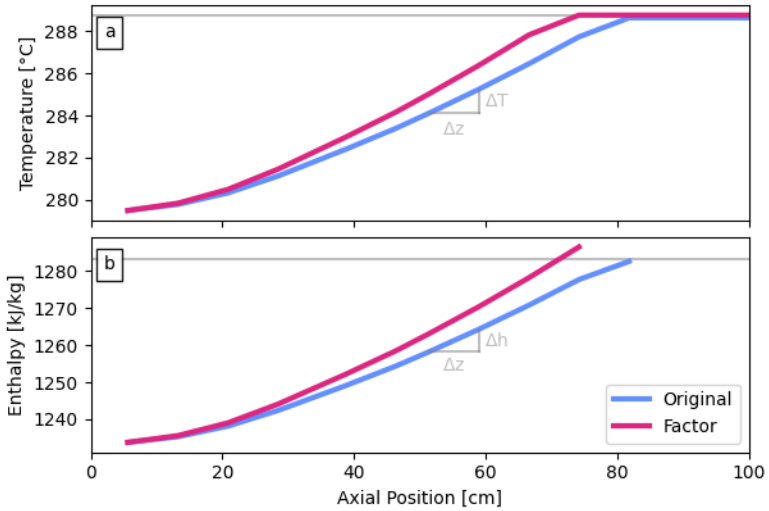

Figure 28. Example of the updated cladding surface temperature of a fuel rod used in the sensitivity study. The multiplier in this example is 1.2.

Note that this algorithm only works if the enthalpy of the rod increases with axial position. This is true during normal operation, but not during the LOCA. Therefore, the algorithm was not applied to the boundary temperature during the LOCA. This should have a negligible effect on the results because the LHR drops to nearly 0 very rapidly during the LOCA.

This change improves the fidelity of the BISON simulations by approximating a feedback effect between LHR and the cladding boundary temperature. However, this is an incomplete analysis. A more detailed

analysis would have run VERA and TRACE simulations using the updated LHRs. However, this formulation should be sufficient to give an idea of the effects of LHR uncertainty on FFRD susceptibility.

6.2 SIMULATION RESULTS

Out of the 2,835 additional simulations, only 7 crashed without finishing. Including the baseline simulations, this is a successful simulation rate of 99.8%. This is a marked improvement in BISON's robustness. In 2022, the successful simulation rate was 276 out of 281 simulations, or 98.2% [1]. Once again, BISON predicted no cladding bursts in any of the rods with 5%, 10%, or 15% higher LHRs.

6.2.1 Analysis Based on Intermediate TRACE Results

For the sake of developing correlations between parameters of interest and cladding burst, as well as to demonstrate that the cladding burst correlations were functioning correctly, an intermediate version of the TRACE simulations with erroneously high temperatures among high-burnup rods was used to develop the BISON simulations and perform the analysis.

The trend of outer surface PCT versus rod average power factor from the earlier version of the TRACE results is shown in Figure 29. This version had realistic power distributions for the rods of interest but there was an issue impacting the power applied to the remaining rods in each assembly. This impacted the heatup and vaporization rate of the coolant within the assembly and led especially to unrealistically high cladding temperatures in some of the peripheral twice-burned assemblies. These can be noted as outliers in the upper left region of the figure. These rods, due to their very high burnup and high temperature, had an increased likelihood of cladding burst in BISON for these earlier TRACE results.

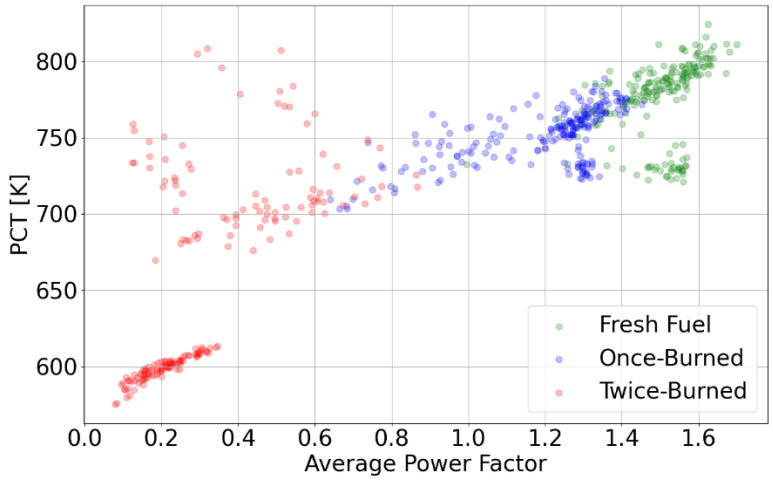

Figure 29. Trend of outer surface PCT versus rod average power factor from the earlier version of the TRACE results.

This set of simulations included 945 rods, for a total of 3,780 simulations once the LHR increases of 5, 10, and 15% are included. 27 simulations crashed, for a completion rate of 99.3%. The CC predicted zero bursts in the nominal case, zero bursts when the LHR was increased by 5%, two rod bursts when the LHR was increased by 10%, and seven when the LHR was increased by 15%. The SRC predicted zero bursts in the nominal, 5%, and 10% cases, and four bursts in the 15% case.

Seven predictions of interest were selected to measure the correlations between the predictions and cladding burst predictions:

- Rod-average burnup,
- FGR,
- Peak hoop strain,
- Peak hoop stress,
- Peak cladding temperature,
- Peak fuel temperature, and
- Plenum pressure.

Since cladding burst predictions are a Boolean value, the point-biserial correlation coefficient (PBCC) was used to quantify the correlation strengths. The cladding burst was converted to an integer value (0 for false, 1 for true) and compared to the end-of-cycle value of each prediction of interest. P-values were calculated to determine the statistical significance of the correlation. The statistically significant (P-values less than 0.05) correlations are shown in Table 6.

Table 6. PBCC and P-values for the cladding burst predictions among simulation sets that included rod bursts. Only statistically significant correlations (P-values less than 0.05) are shown.

LHR Increase	BISON Prediction	PBCC	P-Value
Chapman Correlation			
10%	FGR	0.077	0.018
	Hoop Strain	0.096	0.015
	Fuel Temperature	-0.067	0.039
15%	Average Burnup	0.089	0.006
	FGR	0.124	0.000
	Hoop Strain	0.125	0.000
	Plenum Pressure	0.111	0.001
Strain Rate Criterion			
15%	Average Burnup	0.075	0.021
	FGR	0.093	0.004
	Hoop Strain	0.125	0.000
	Cladding Temperature	-0.072	0.027
	Fuel Temperature	-0.084	0.010

The hoop stress was the only value to not have a statistically significant correlation to cladding burst in at least one of the burst correlations. This may be due to creep reducing the stress during normal operation. Average burnup was correlated to both correlations in the 15% cases. FGR and hoop strain were correlated in all three cases. The peak cladding temperature had a negative correlation to the SRC, and the peak fuel temperature had negative correlations to the CC in the 10% case and the SRC. The plenum pressure was correlated to the CC in the 15% case. In all three sets (CC-10%, CC-15%, and SRC-15%), the strongest, most statistically significant correlation is with hoop strain.

The assembly locations of bursts are also of interest. These are shown in Figure 30. No assembly saw more than a single rod burst in either burst model or LHR factor. Additionally, the bursts were concentrated at the core periphery, where the erroneous cladding temperature, twice-burned rods were concentrated. No bursts were predicted among the HBLUAs.

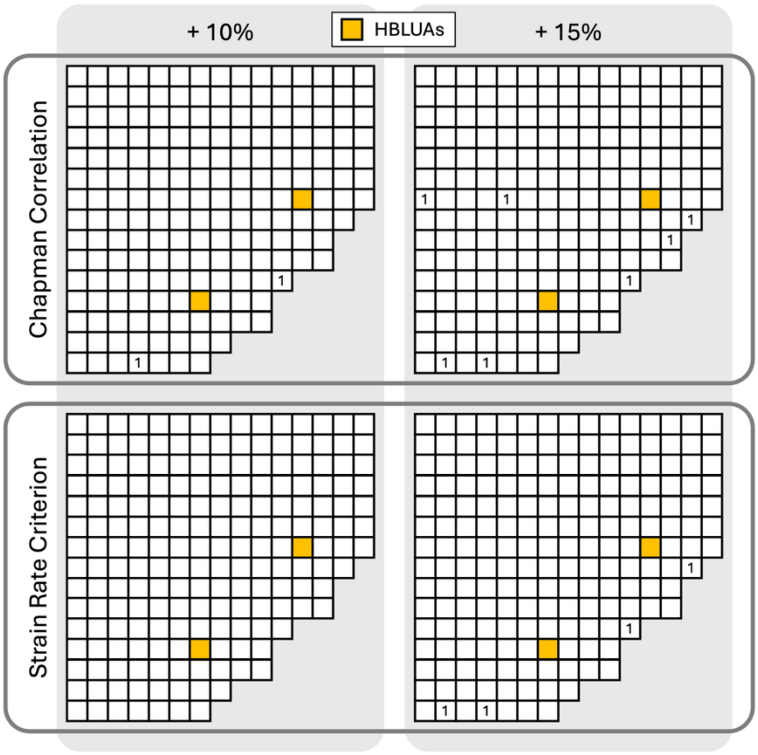

Figure 30. The number of burst rods per assembly according to the burst model and the LHR increase. The HBLUAs are marked yellow.

6.3 DISCUSSION

Even after increasing the LHR by 15%, BISON predicted no cladding bursts in any of the 945 rods simulated. However, by using intermediate TRACE data with erroneously high temperatures, failures were obtained, and correlations were able to be developed. The temperature correlations are the most surprising results. The peak fuel temperature is correlated to the CC when the LHR is increased by 10%, but not when it is increased by 15%. In addition, all temperature correlations are negative. Considering that the CC is a temperature-based correlation, this is unexpected. This is almost certainly a secondary effect due to temperature's correlation with burnup. The fact that bursts did not occur in the simulation set with lower, more accurate temperatures, is evidence that this is the case.

The burnup and peak cladding temperature are compared for the SRC model with a 15% LHR multiplier in Figure 31. A comparison with the groupings in Figure 19b shows that all bursts occurred within twice-burned rods, which lends credence to the theory that the temperature correlation is an artifact of the burnup correlation.

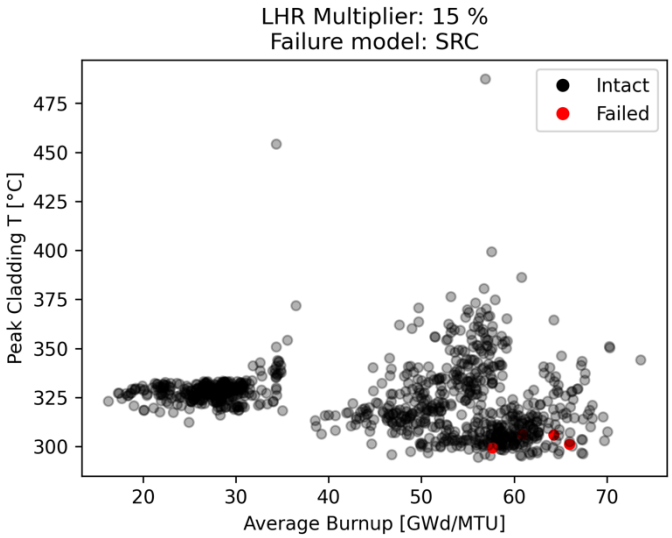

Figure 31. Comparison of end-of-cycle burnup and peak cladding temperature predictions when the LHR is increased by 15%. The data are colored according to the burst status according to the SRC.

In both the CC and SRC cases, the two strongest correlations, both in terms of PBCC and P-value, are the FGR and peak hoop strain. These two values are plotted together in Figures 32 and 33 for the CC and SRC bursts, respectively. The figures show that the FGR and strain are correlated to one another, which means at least part of the correlation to cladding burst is a secondary effect. In addition, they show that while the FGR and hoop strain are correlated to burst, these two values alone do not necessarily predict burst. The rods with the highest FGR and strain are not predicted to burst. The FGR predictions far exceed the corresponding predictions with the updated TRACE data. This is likely caused by the LHR multiplier raising the fuel temperature. Temperature has an exponential effect on fission gas diffusion, which can drastically increase the FGR predictions.

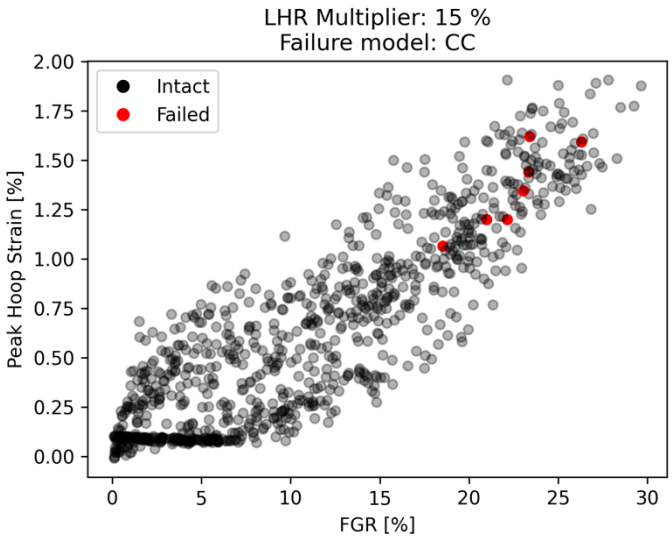

Figure 32. Comparison of end-of-cycle FGR and peak hoop strain predictions when the LHR is increased by 15%. The data are colored according to burst status according to the CC.

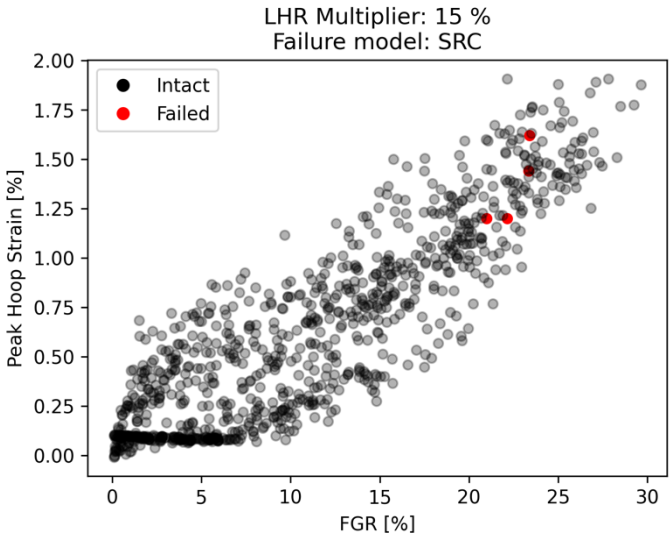

Figure 33. Comparison of end-of-cycle FGR and peak hoop strain predictions when the LHR is increased by 15%. The data are colored according to burst status according to the SRC.

It must be emphasized that the results presented here are based on erroneous results with high TRACE-predicted temperatures. The simulations with the most accurate assumptions and models predicted that no rods would burst, even with a 15% increase in the LHR. However, these results are not predictive and should not be used as safety-basis calculations. Future work should expand the sensitivity and uncertainty analysis to include all three codes, include recently updated BISON BWR models, and continue to expand the timeframe of the TRACE simulations.

7. TRACE AND CTF BENCHMARK

While TRACE was solely used for setting the transient LOCA boundary conditions in BISON, it was determined that a benchmark against CTF would be of value to assess potential variation in the solution, to exercise CTF for LOCA conditions, and to check the agreement of CTF with TRACE because it is the T/H solver used in the VERA code. A similar benchmark study was performed in a past milestone, but for PWR cores [15]. This study seeks to perform a similar analysis for BWR cores. Furthermore, this study expands the analysis by modeling the blowdown phase of the LOCA, whereas the previous PWR study only modeled the reflood portion. The lumped model (coarse mesh) benchmark was successfully completed; however, it was not possible to complete a rod-resolved analysis in CTF at this time. The rod-resolved model was set up, but convergence difficulty prevented running the full transient. Large, local pressure spikes were encountered during the blowdown phase of the transient that required prohibitively small timestep sizes. Additional development work will be needed to add support for blowdown modeling in rod-resolved models.

7.1 DEVELOPMENT OF TRACE AND CTF CORE MODELS

To simplify the analysis, two assemblies were selected for the benchmark: a high-burnup HBLUA and a once-burned assembly (once-burned at beginning of Cycle 18). The once-burned assembly was selected because it was the highest burnup assembly among the interior “checkerboard” assemblies at the end-of-rated statepoint. This ensured it had relatively high assembly-average burnup (45.6 GWd/MTU at the end-

of-rated statepoint) while also having higher-than-average power (an assembly power peaking factor of 1.21). The high-burnup HBLUA had an assembly-average burnup of 55.4 GWd/MTU and an assembly power factor of 0.57 at end-of-rated. The assembly power was obtained from end of Cycle 18. The once-burned assembly was at Row 18, Column 16 in Figure 34 and the high-burnup assembly was at Row 27, Column 22.

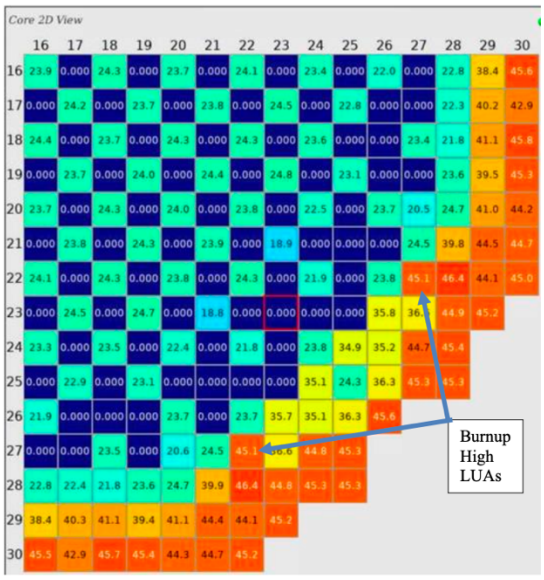

Figure 34. Beginning of Cycle 18 core loading map.

In the TRACE system model, conduction through the channel box to the bypass was not modeled. Therefore, it is possible to simplify the benchmark by only modeling these individual assemblies instead of the entire core if the system code solution is used to set the inlet and outlet boundary conditions of the individual assemblies. Results for liquid and vapor mass flow rate were printed at the assembly inlet plane as well as liquid and vapor temperature, vapor void, and pressure for the inlet plenum volume to determine inlet boundary conditions. The transient pressure solution, as well as liquid and vapor temperature and vapor void were also printed for the outlet plenum volume to determine outlet boundary conditions.

Two single-channel TRACE and CTF models were built to model the two assemblies. A simple schematic of an assembly model is shown in Figure 35.

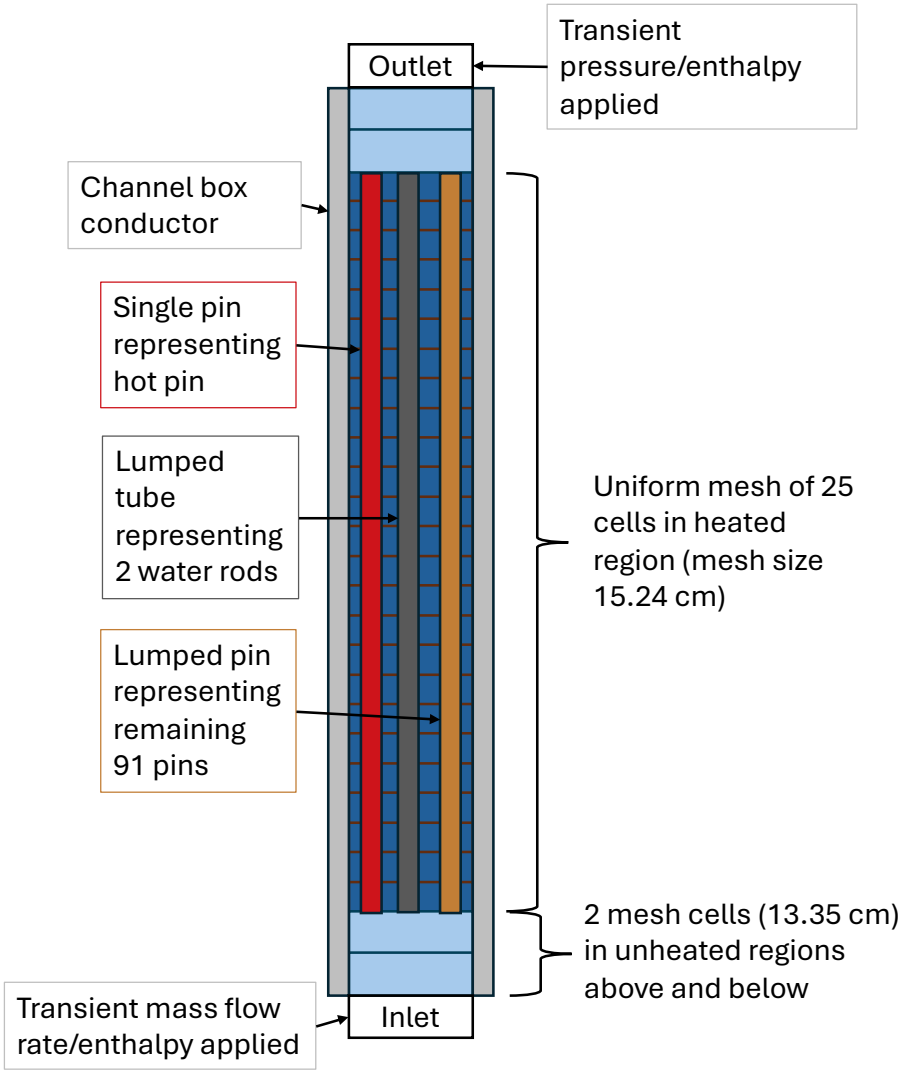

Figure 35. Schematic of the lumped modeling approach used in CTF and TRACE.

The assembly includes a lower and upper unheated region and a central heated region. The flow area and wetted perimeter were varied along the axial length to account for the presence of axially varying water rods and part-length rod termination.

Four conductor objects are used in the model, including an object for the hot fuel rod, one lumped object to represent the other 91 fuel rods, one to represent the channel box, and one lumped tube object to represent the two water rods. Note that part-length rods are lumped into the average rod and the lumped power is adjusted to account for their presence and to conserve total energy. It must be noted that the TRACE model includes flow inside of the water rod object, whereas the CTF model has an adiabatic boundary condition. The models could not be made consistent in this regard, so a sensitivity analysis is later performed to show that this difference has an insignificant impact on the solution. Both the CTF and TRACE models apply an adiabatic boundary condition on the outside of the channel box. Note that the material properties for stainless steel 304 were used for modeling of the channel box, although the actual material was zircaloy. The difference in material properties is not expected to significantly impact the results, and more importantly the TRACE and CTF assumptions were consistent (both assumed stainless

steel 304). The material properties can be found in the TRACE Theory Manual [7]. The advanced dynamic gap fuel rod model was enabled in both codes.

Spacer grid form loss coefficients were also applied at the levels nearest to actual spacer locations in the core. The form loss coefficient values were identical between CTF and TRACE and matched the values given for GNF2 fuel. Note that TRACE internally calculates a form loss coefficient for a sudden area expansion or contraction. CTF uses a Borda-Carnot approximation for estimating the loss, so there may be differences in how pressure drop near the part-length rods is determined; however, it is anticipated this will have a minor effect due to the generally low velocities in the bundle during these conditions.

The TRACE full system solution can be directly used in the TRACE single channel models; however, CTF requires the mixture enthalpy for a two-phase mixture. The liquid and vapor enthalpy was calculated using the TRACE pressure and temperature of the liquid and vapor throughout the transient. A mixture enthalpy was calculated by void weighting the void and liquid enthalpy in the inlet and outlet volumes. The inlet plenum occasionally achieves high void, but due to the large density difference, the liquid enthalpy always dominates the inlet mixture enthalpy. The outlet mixture enthalpy is also calculated and applied in the event that a flow reversal at the outlet plane occurs. A comparison of inlet enthalpy is later made between the two models to ensure that the inlet boundary condition is consistent.

The inlet flow rate calculated by the TRACE full system solve included significant oscillations in time starting around 100 s and these tended to cause stability issues in the CTF solution. To mitigate this, a simple moving average filter with a window size of 10 datapoints is used to smooth the boundary condition before applying it to the single channel TRACE and CTF models. This filter is only applied between 75 and 156 s, where the data are oscillating. In addition to the filter, reverse inlet flow was set to a floor value of 0 kg/s because severe, quick flow reversals were also found to be problematic. As these oscillations were short-lived, it was anticipated that it would have minimal impact on the solution behavior. This filtering leads to the following smooth transient behavior (orange line) compared to the original data (blue line) shown in Figure 36.

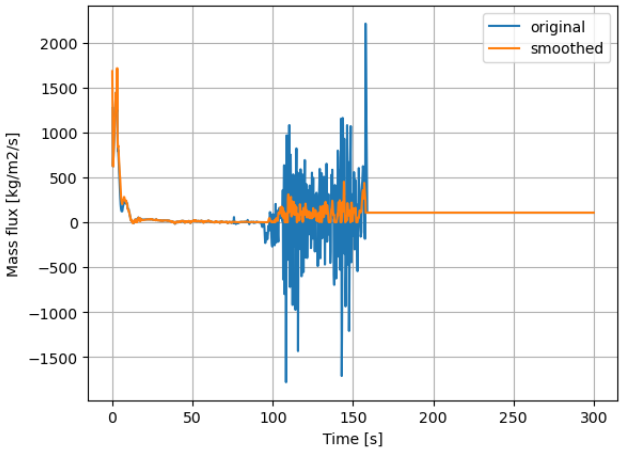

Figure 36. Smoothing function applied to transient inlet mass flow rate.

The final model parameter needed is the bundle power and rod power distribution. This was obtained from the EOC power distribution predicted by VERA for Limerick, Cycle 18. The hot-rod axial power distribution was directly copied from the VERA output file. The lumped-rod power distribution was calculated by performing a straight average of the power factors for all rods that are captured by the lumped rod. Note that, when part-length rods terminate, their power factor becomes zero and brings the overall average value down. Ultimately, bundle power is preserved in this way, and it is verified that both

CTF and TRACE receive the same absolute power in their models. Figure 37 shows the hot rod and average rod profiles applied to the hot assembly model. The same is shown for the high-burnup assembly in Figure 38.

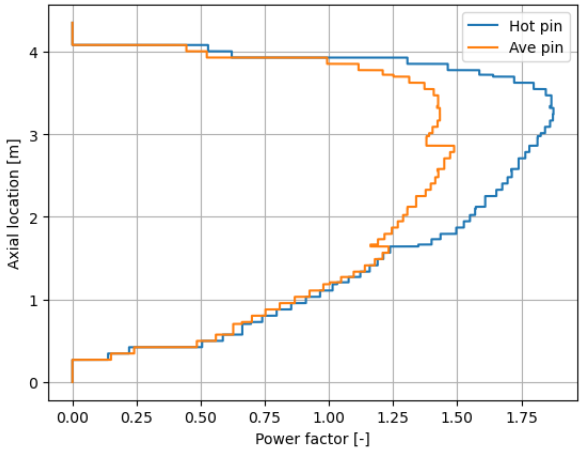

Figure 37. Power profile of hot and average rods in the hot assembly lumped model.

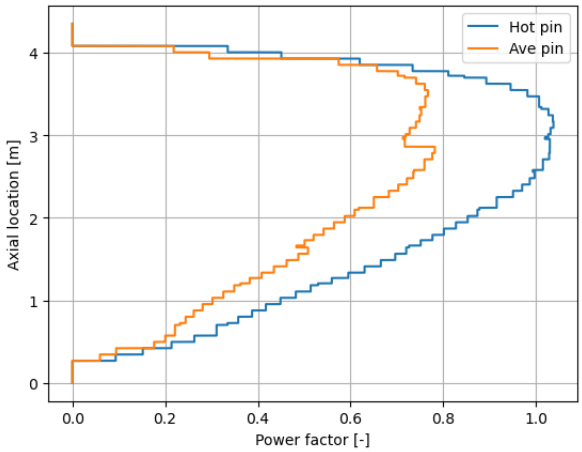

Figure 38. Power profile of hot and average rods in the high-burnup assembly lumped model.

The water rods are not included in the lumped rod average, as they have their own object to capture their behavior. In addition to the rod power data, the rod burnup solution was copied in the same way. The rod burnup will impact the fuel pellet conductivity in both CTF and TRACE models. A transient power ramping factor was applied to both codes to represent the power decrease due to the shutdown and decay heat.

7.2 CTF BOUNDARY CONDITION MODIFICATION

The standard CTF boundary condition input accepts total inlet mass flow rate and mixture enthalpy as an input. The inlet void is calculated assuming zero phase slip given this information. This can lead to inconsistency with the TRACE boundary values, which will have slip. This can lead to differences in total inlet enthalpy injection. Furthermore, even though both codes use IAPWS97 for fluid properties, small implementation differences can lead to differences in saturation temperature and big changes to void between the two codes. To eliminate all possible sources of boundary condition discrepancy, CTF was

modified to add a custom reader that will read a time-dependent table of liquid mass flow rate, vapor mass flow rate, liquid enthalpy, vapor enthalpy, and vapor void at the inlet as well as a time-dependent table of pressure, liquid enthalpy, vapor enthalpy, and vapor void at the outlet. These values are directly set to the CTF boundary values rather than making assumptions about phase slip and determining void from mixture enthalpy. As will be shown later, this leads to excellent agreement between the codes on boundary solution values.

7.3 BENCHMARK OF LUMPED MODEL

Sanity checks are first performed for the inlet and outlet conditions printed by CTF and TRACE to ensure that the models are, in fact, consistent. Both the hot and high-burnup assemblies connect to the same lower and upper plenum volumes, so the boundary conditions only need to be verified for one of the assemblies. Figure 39 through Figure 42 show the CTF and TRACE reported liquid mass flow rate, vapor mass flow rate, mixture enthalpy, and outlet pressure. All figures show excellent agreement with the exception of four times in CTF when the inlet mixture enthalpy spikes. Note that the mixture enthalpy is calculated as a mass flow rate weighted value. While the liquid and vapor mass flow rates match well with TRACE, the inlet enthalpy will be limited to saturation values, which can vary based on CTF calculated pressure in the inlet plane.

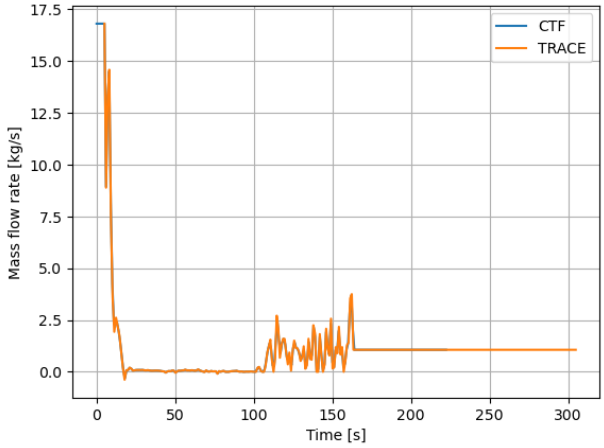

Figure 39. Liquid mass flow rate at inlet plane in TRACE and CTF.

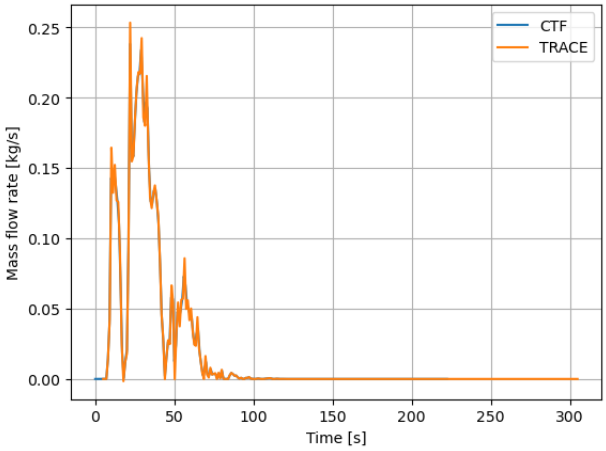

Figure 40. Vapor mass flow rate at inlet plane in TRACE and CTF.

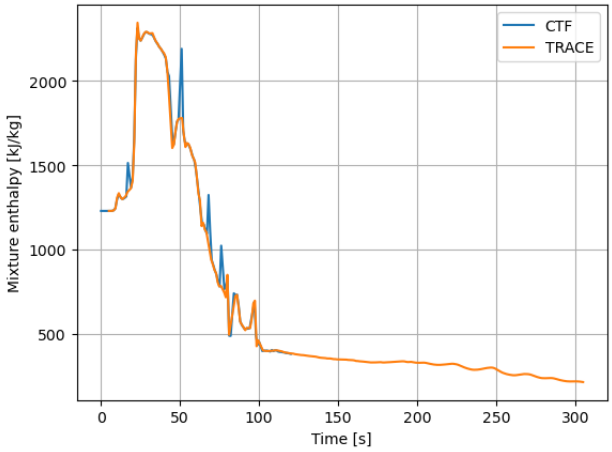

Figure 41. Mixture enthalpy at inlet plane.

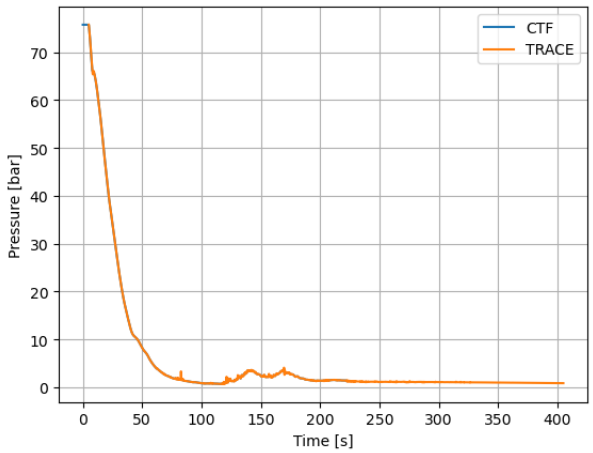

Figure 42. Pressure in outlet control volume in TRACE and CTF.

7.3.1 Hot assembly

The results for the once-burned, hot assembly are shown in this section. Note that the CTF simulation crashed due to failure to reduce timestep at around 220 s. The cause of the repeated timestep failures was due to a combination of pressure going out of bounds and vapor becoming too subcooled. Despite the crash, the most important portion of the transient was completed successfully.

First, the quench front location is printed for both the hot and average rods in Figures 43 and 44, respectively. Little difference is observed between the hot and average rods. The assembly uncovery rate matches well, as does the lower extent of the dryout location. CTF does tend to quench faster than TRACE. This matches the behavior observed for the PWR LOCA benchmark study, where CTF also quenched faster in those cases [15].

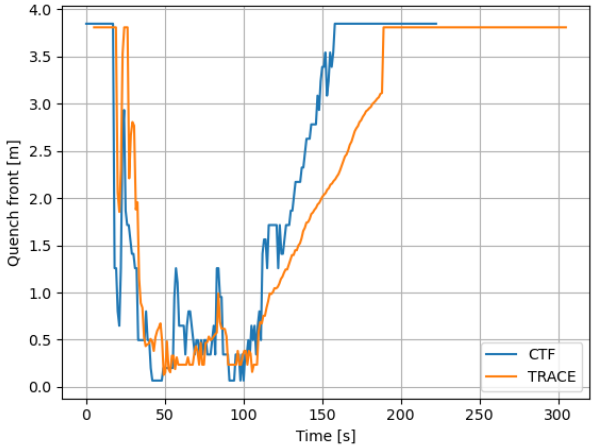

Figure 43. Quench front location for hot rod in hot assembly.

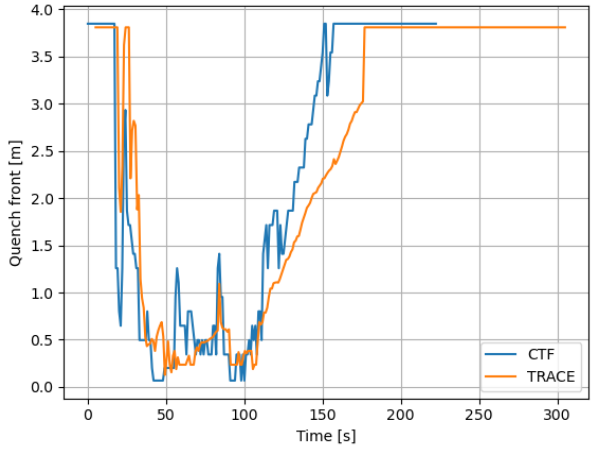

Figure 44. Quench front location in average rod for hot assembly.

To better compare the solutions, selected solution parameters are compared at different axial locations in Figure 45–47. The figures show four plots: hot rod cladding surface temperature (top-left), void fraction (top-right), liquid velocity (bottom-left), vapor velocity (bottom-right). All plots are showing the transient solution response for a given level. At all locations, it is observed that CTF tends to predict dryout more readily than TRACE, but it also predicts faster quench than TRACE. As a result, CTF tends to predict several short-lived dryout events that do not reach a high outer surface PCT. The exception is near the top of the bundle, where TRACE predicts a much less severe temperature excursion than CTF. This may be due to upper head safety injection, which is not being properly captured in CTF.

Aside from the temperature response, void collapse tends to match quite well for the lower and middle areas of the bundle. In the upper portion, TRACE never fully collapses the void. CTF does collapse it around 150 s, but then it increases suddenly again near 170 s. Both codes observe this sudden increase in void as low as 3 m in the bundle, but it quickly collapses again. Referring to the power profile plot in Figure 37, it is observed that power is highest in the upper portion of the bundle and may be the cause of the void excursion observed in this location. The high power may lead to an increased vapor generation rate.

Focusing on the velocity profiles, it is observed that TRACE predicts much higher vapor slip in its pre-CHF flow regimes, as vapor velocity is much higher in TRACE near the end of the transient, but only in the lower and middle bundle portions, which should be bubbly or slug flow regimes. Also, the vapor velocity trend tends to agree quite well between the two codes, which is not always true for the liquid behavior. It is interesting that both TRACE and CTF are susceptible to large spikes in the vapor velocity at roughly the same locations in space and time. For example, near the top of the bundle, there is a strong spike in both liquid and vapor velocity at around 75 s. This has the effect of increasing heat transfer enough to quench the rod at that location in both codes. Once the spike drops, the rod dries out again in both codes. This appears to be due to a pressure spike that propagates through most of the bundle at around 75 s (see Figure 48). It is not clear where this spike comes from, as it is not applied at the outlet boundary condition. The spike is felt by both codes; although, the CTF spike is more severe. Still, the TRACE liquid and vapor velocity spike in response to this pressure spike is just as severe as the CTF velocity spikes.

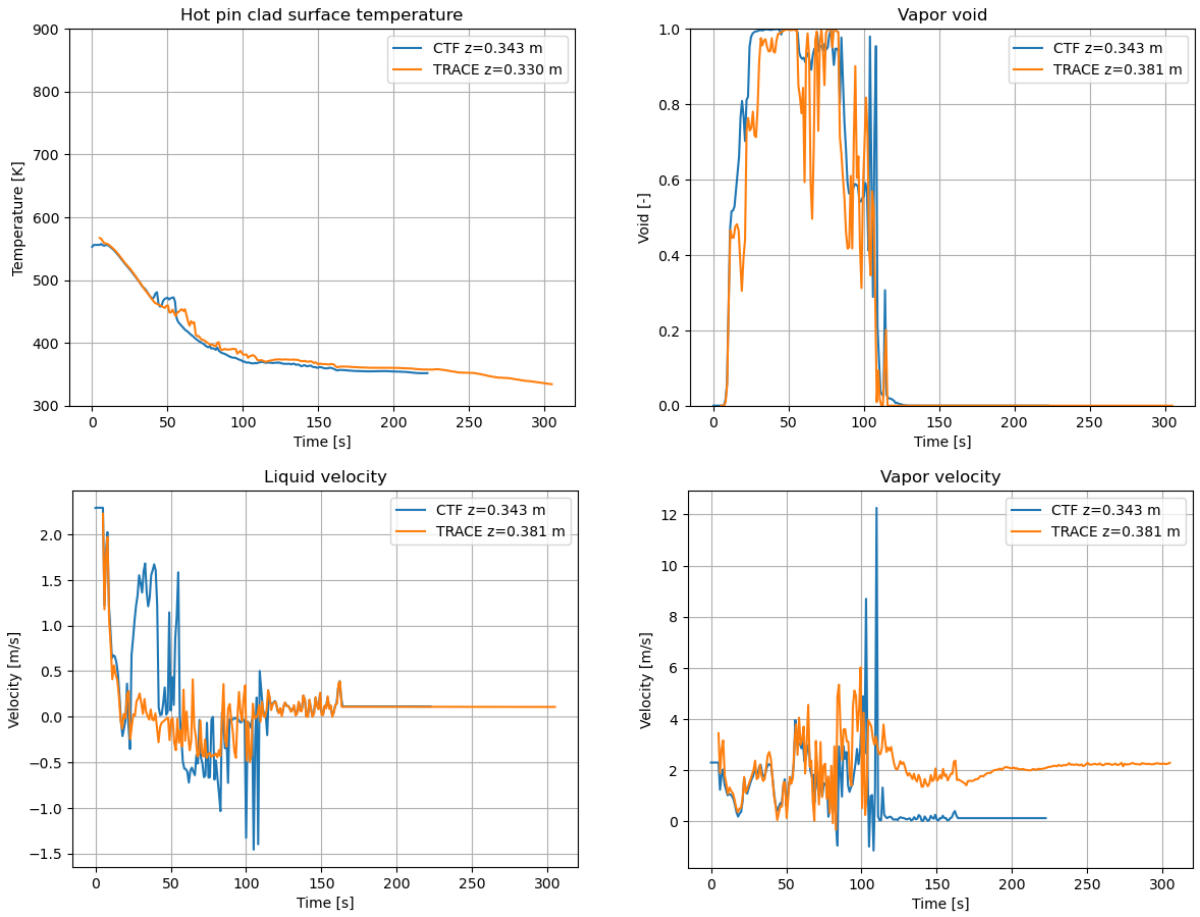

Figure 45. CTF and TRACE solution for hot assembly near bottom of bundle.

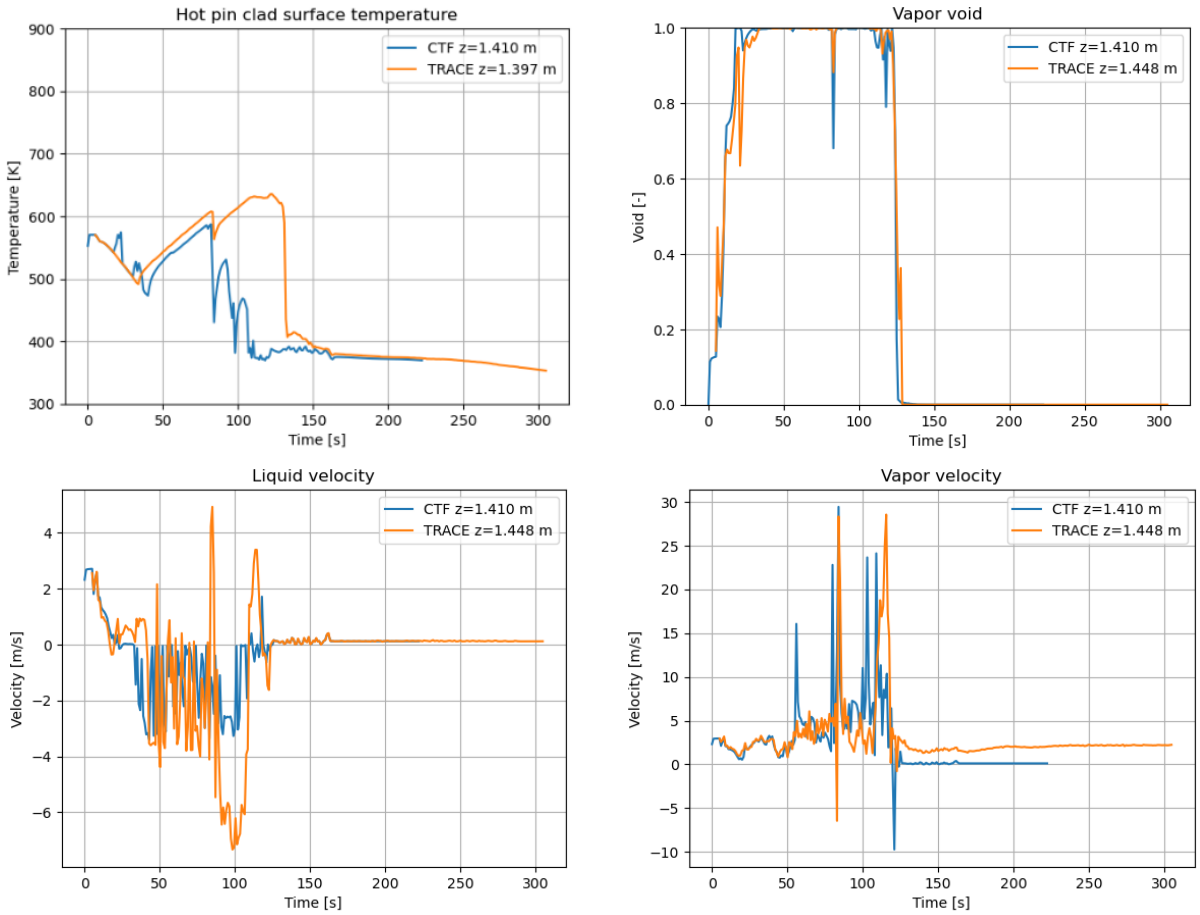

Figure 46. CTF and TRACE solution for hot assembly near middle of bundle.

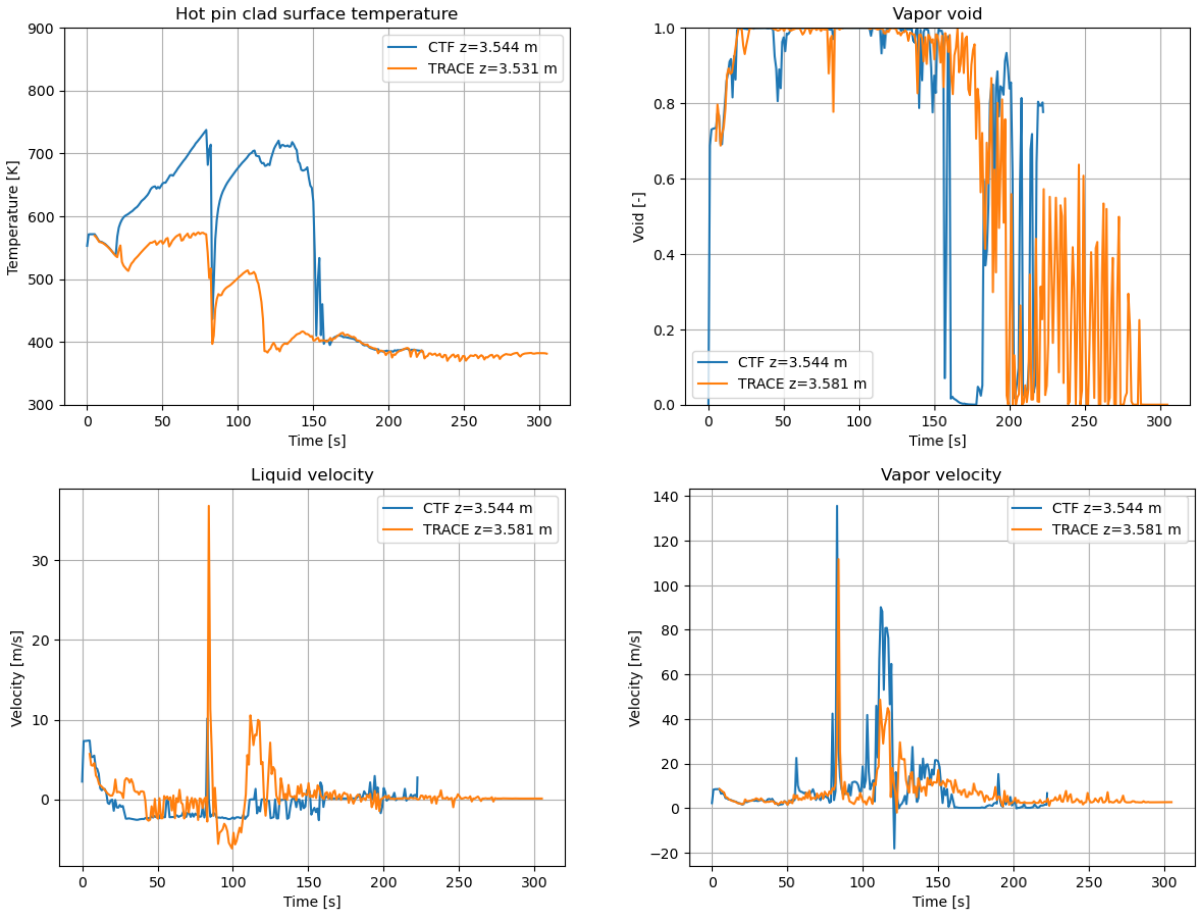

Figure 47. CTF and TRACE solution for hot assembly near top of bundle.

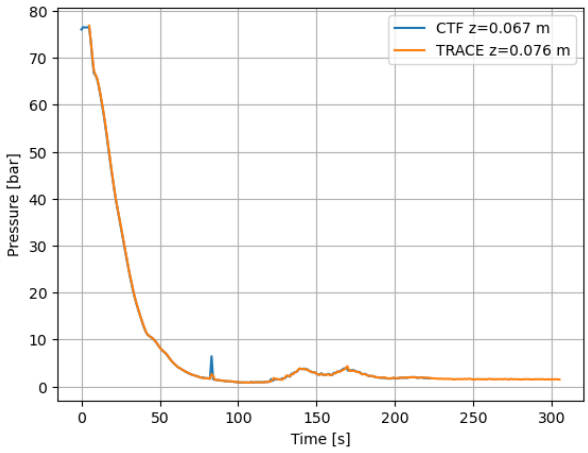

Figure 48. Transient pressure behavior near bottom of bundle in the hot assembly.

The average rod behavior is similar to the hot rod behavior, so it is not shown. There are some differences in temperature behavior of the channel box and water rod that is worth investigation. Figures 49 and 50

show the temperature behavior at mid- and upper-bundle locations respectively as well as heat transfer behavior in CTF. Both TRACE and CTF predict intermittent dryout of the unheated objects; however, CTF predicts more prolonged dryout events that show up as plateaus in temperature. This is opposite to the heated conductor behavior, which tends to experience shorter-lived dryout events in CTF. Additionally, the unheated conductors tend to reach much higher temperature in CTF during the dryout events.

It can be seen in the fluid temperature plots that the vapor is superheated in both codes between 25 and 125 s. In the mid-bundle location, TRACE achieves higher superheat, but in the upper-bundle location, CTF achieves the higher superheat. Similar to the upper-bundle quenching behavior, this is likely due to mistreatment of upper head injection in the CTF model. Note that the prolonged dryout events in the CTF model correspond to when the bundle is still fully uncovered. At 125 s, void has collapsed in most of the bundle and the majority of the bundle has quenched. The heat transfer coefficient (HTC) plots show the HTC behavior for the three modes of heat transfer in CTF (heat transfer to the liquid, heat transfer to the liquid due to boiling, and heat transfer to the vapor). The plateau and temperature excursion events occur when the vapor heat transfer is the only mechanism of heat removal. This would primarily be vapor convective heat transfer with some radiative heat transfer effects, but heat transfer due to things like droplet impingement or boiling due to intermittent surface contact would be absent. Perhaps TRACE predicts additional heat transfer due to liquid contact, which would account for the lower channel box temperature.

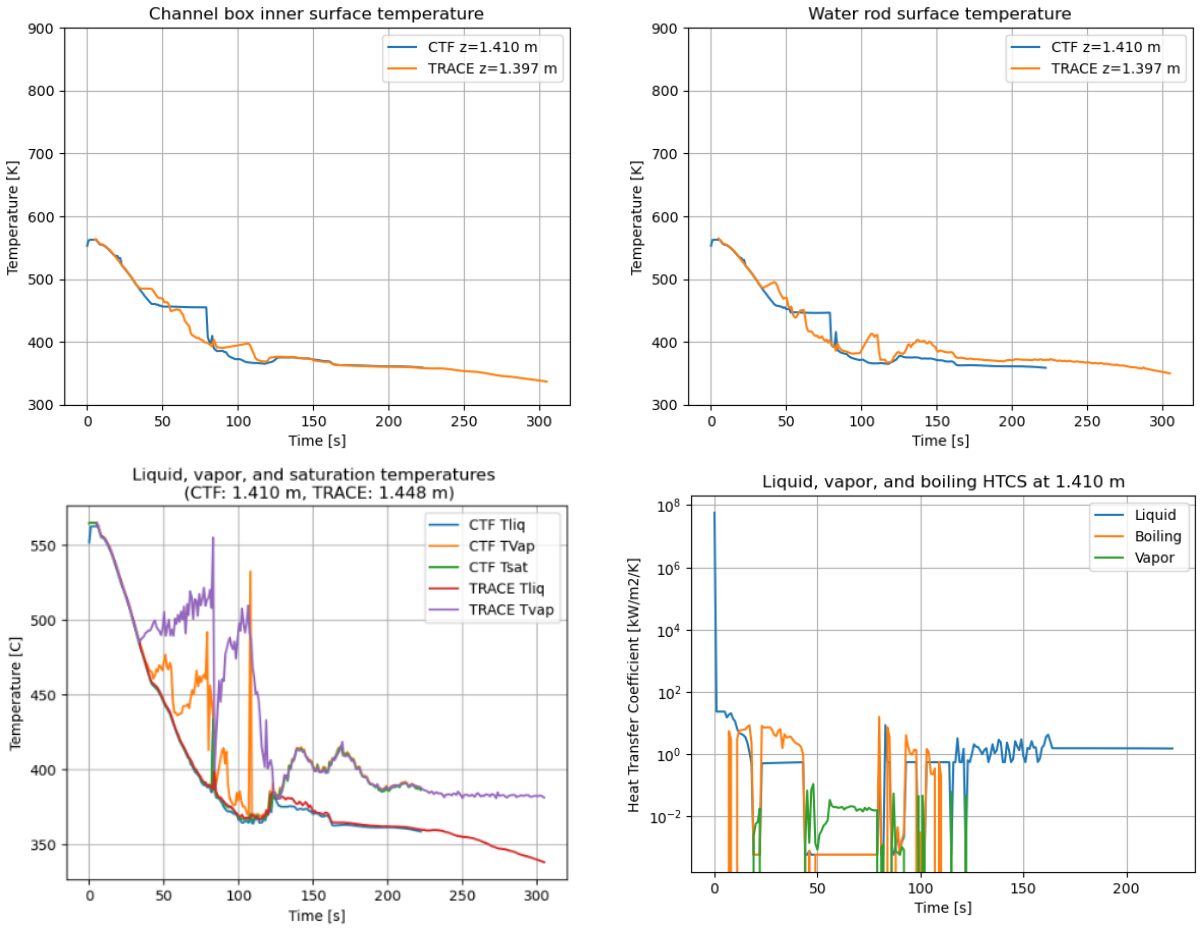

Figure 49. TRACE and CTF solution of unheated object and fluid temperatures for hot assembly near mid bundle.

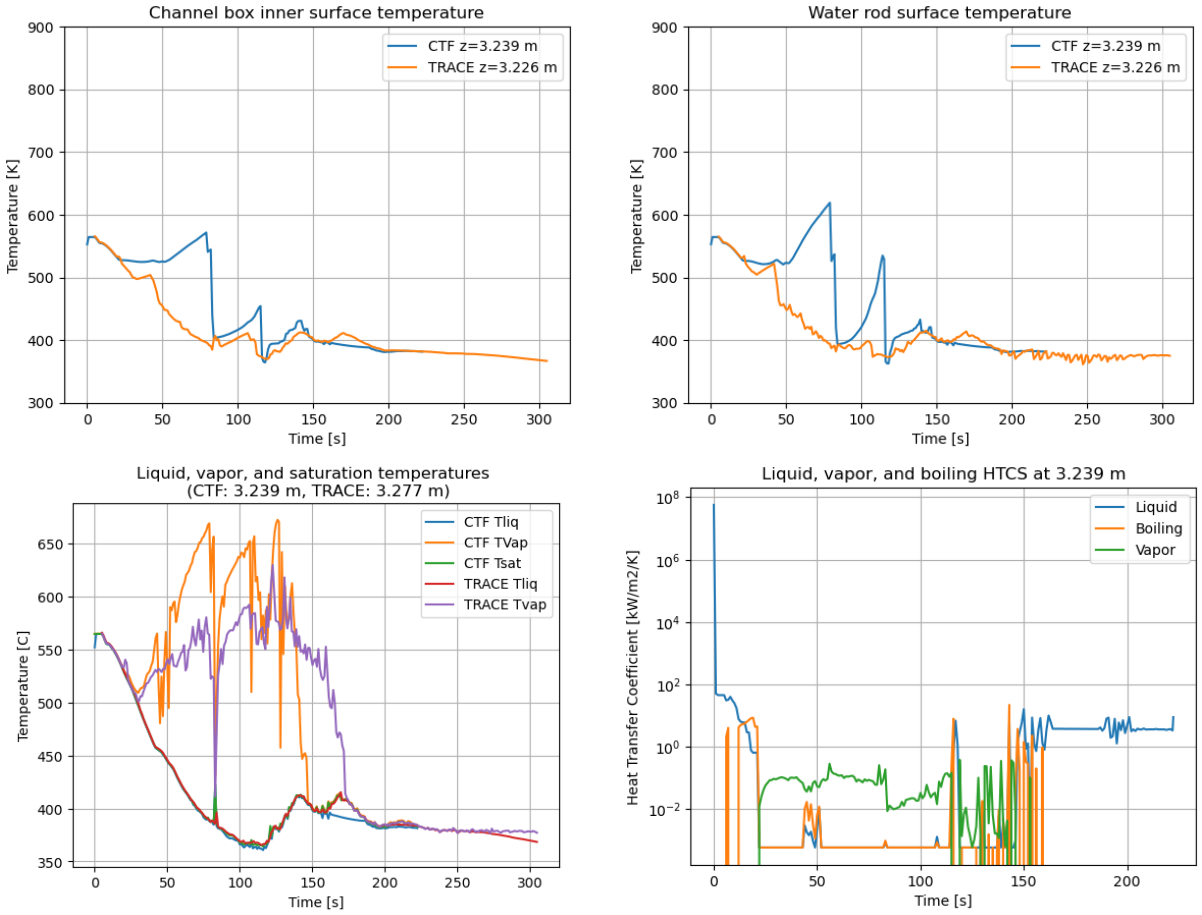

Figure 50. TRACE and CTF solution of unheated object and fluid temperatures for hot assembly near upper bundle.

7.3.2 High-burnup assembly

The high-burnup assembly crashed at roughly the same time in the transient as the hot assembly (231 s vs. 222 s). The quenching behavior for the hot and average rods is shown in Figure 27 and Figure 28, respectively. The quenching behavior in the high-burnup assembly is more consistent between the two codes than it was in the hot assembly. TRACE predicts a quench time that is almost 50 s earlier in the high burnup assembly. CTF predicts a quench time that is only about 20 s earlier in the high burnup assembly.

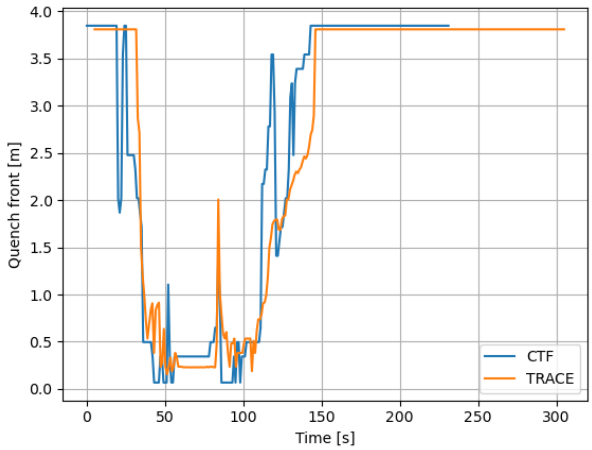

Figure 51. Quench front location for hot rod in high-burnup assembly.

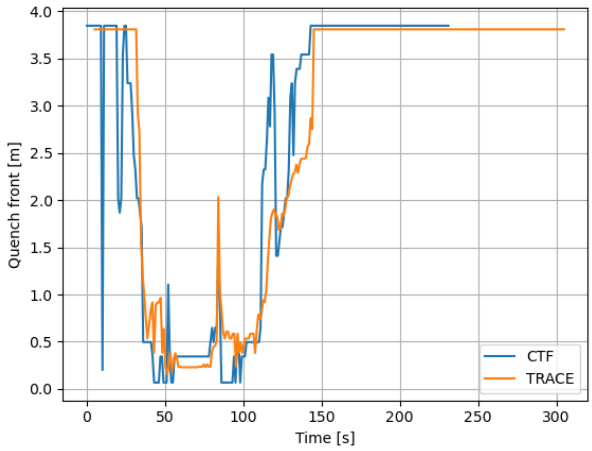

Figure 52. Quench front location for average rod in high-burnup assembly.

The actual rod temperature behavior is similar to the hot assembly, as shown in Figure 53 and Figure 54. CTF continues to predict quicker re-wet and many axial locations see CTF predicting earlier dryout. The upper bundle portion is still over-predicted by CTF. The void collapse timing agrees very well between the codes. In the case of the high-burnup assembly, it does not see the excessive oscillation in void in the top of the bundle like was observed in the hot assembly, though there are still some void excursions that are quickly terminated. Both codes predict these void excursions. TRACE continues to predict higher vapor velocity after the quench. Both codes predict the velocity spikes at the same time as in the hot assembly, indicating the cause of the spike is likely related to the boundary conditions. This spike continues to cause temporary re-wet of the rods.

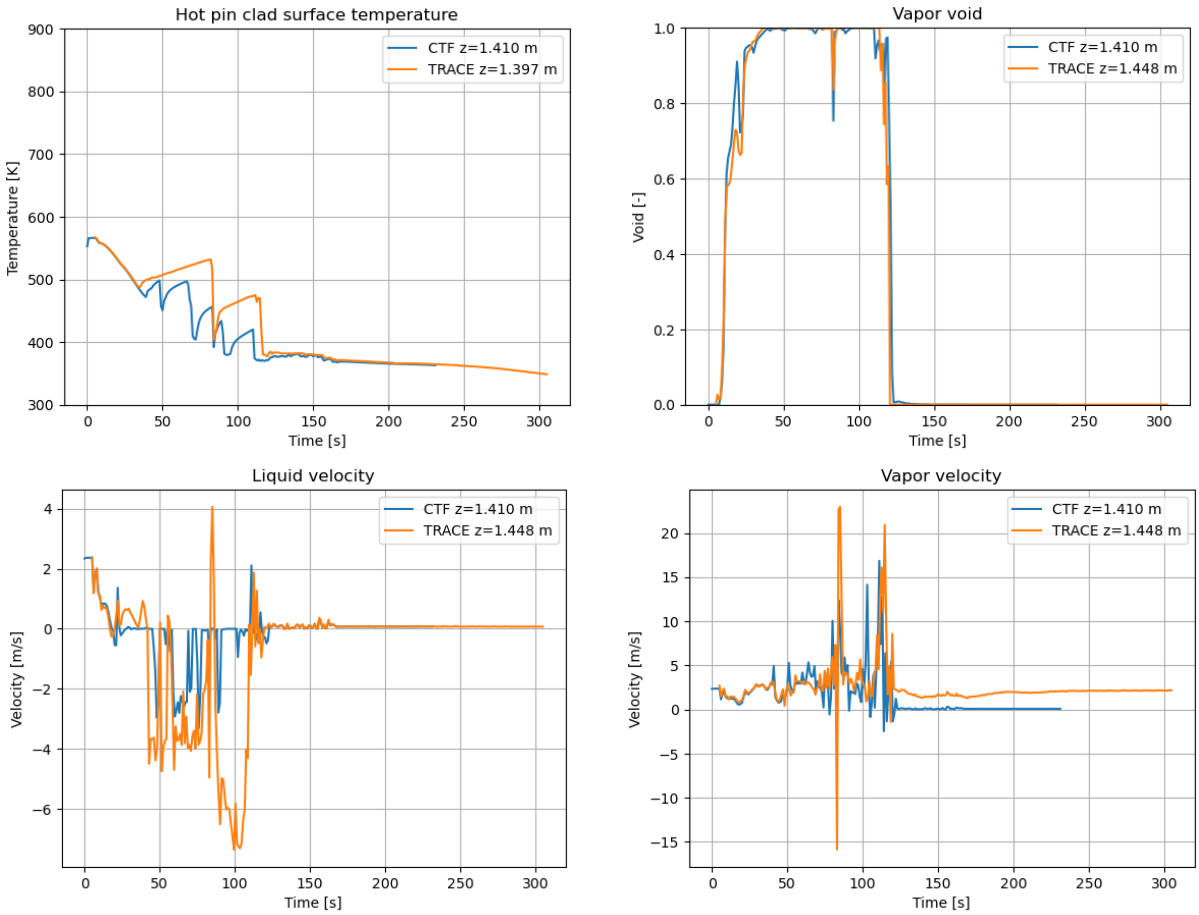

Figure 53. CTF and TRACE solution for high-burnup assembly near middle of bundle.

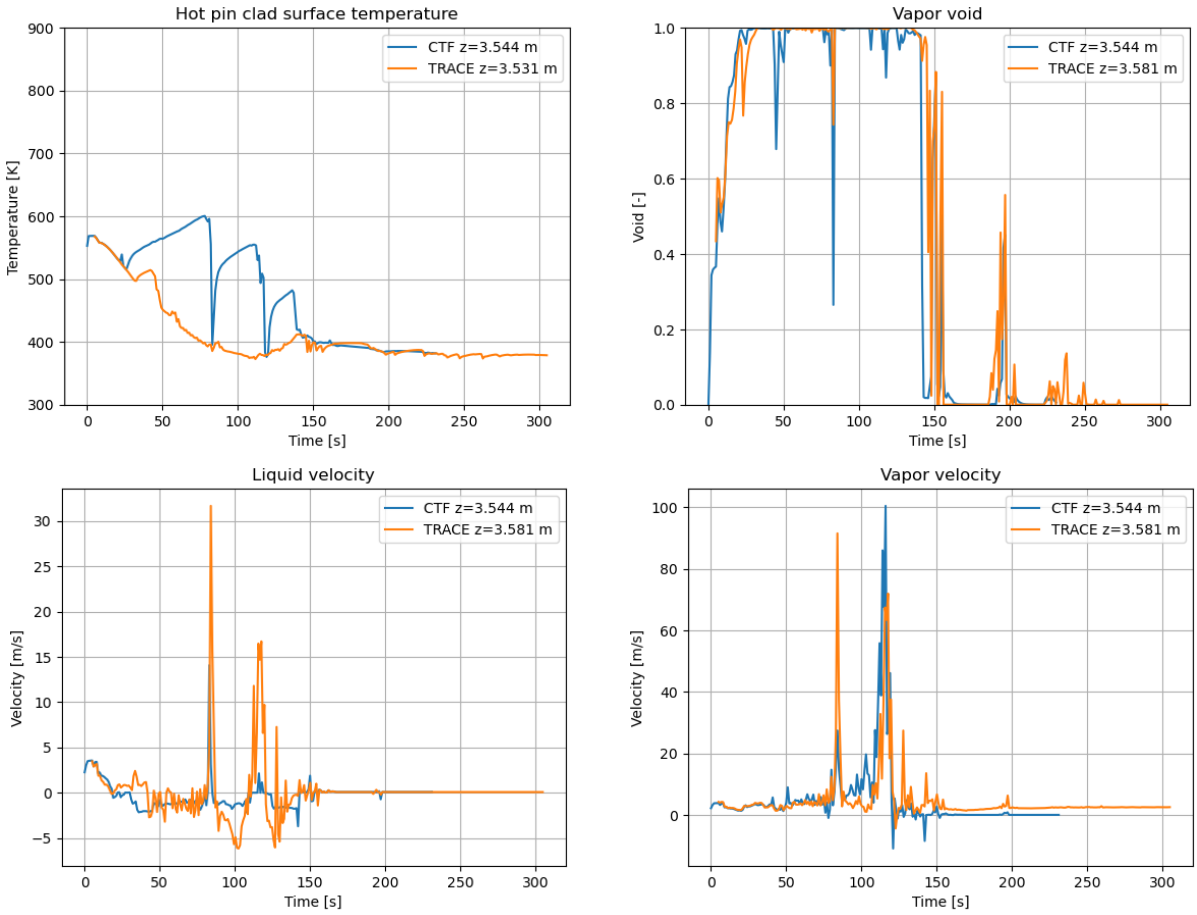

Figure 54. CTF and TRACE solution for high-burnup assembly near top of bundle.

The channel box and water rod behavior, as well as fluid temperature and heat transfer coefficient behavior, is shown in Figure 55. These values are shown more towards the upper end of the bundle. The plateau behavior in the channel box and water rod continues, this time with a distinctive drop at around 80 s. The vapor temperature superheating is roughly the same in CTF and TRACE at this level and both codes predict a sudden drop in the vapor superheat due to the pressure spike at about 80 s. This drop in vapor temperature, along with the brief spike in boiling heat transfer, leads to the rapid drop in temperature of the channel box and water rod.

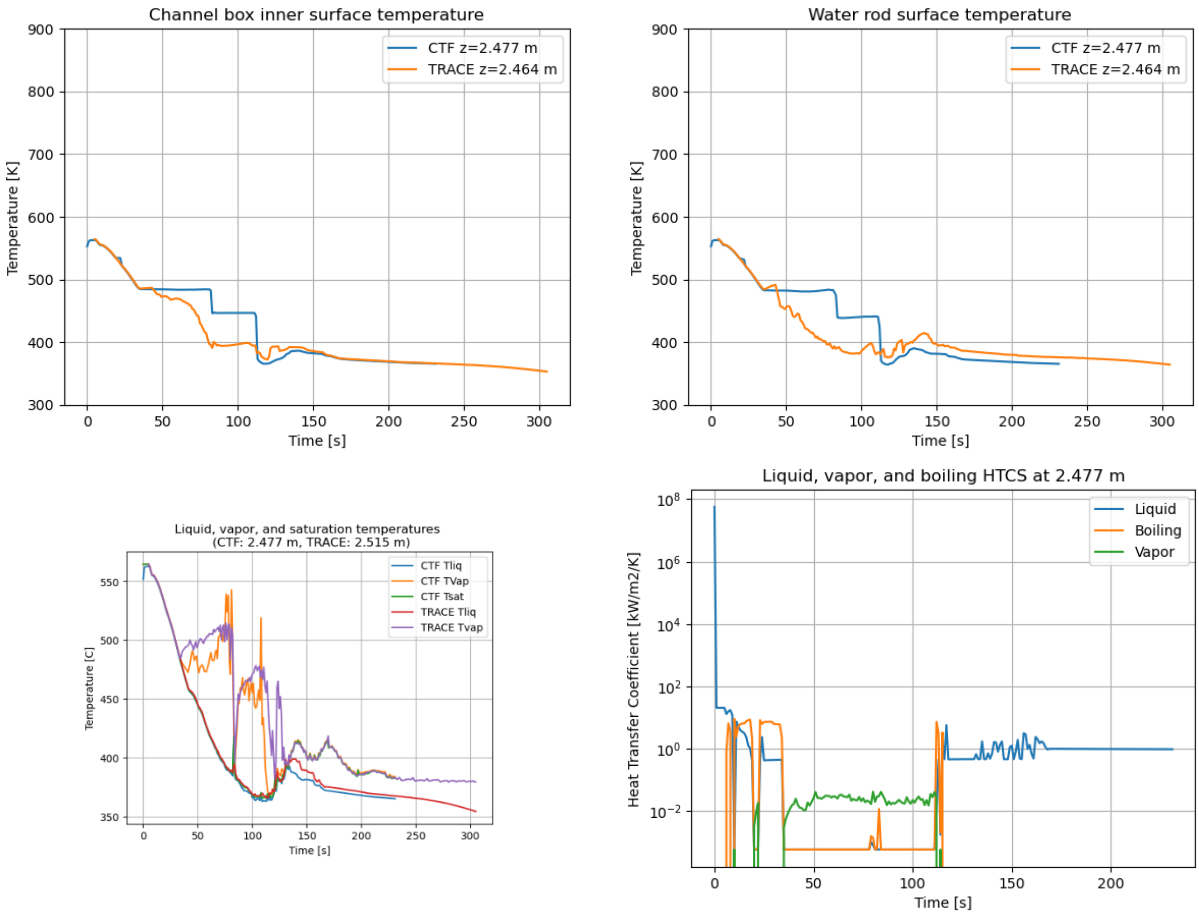

Figure 55. TRACE and CTF solution of unheated object and fluid temperatures for high-burnup assembly near upper bundle.

7.4 TRACE SENSITIVITY STUDIES

As stated previously, TRACE explicitly models flow through the water rods as an additional flow path within the assembly, whereas CTF does not explicitly model this flow. In TRACE, the water rod flow path is connected to the main assembly flow path via junctions at the water rod inlet and outlet axial locations. Each junction is defined by a junction flow area and form loss factor. These were set based on the GNF2 fuel specifications. Convective heat transfer between the main assembly flow, water rod shell, and water rod flow is also modeled in TRACE.

To investigate the impact of water rod modeling on the LBLOCA benchmark results, an exploratory TRACE case was set up in which the water rod inlet and outlet form loss factors were set to 10^6, which vastly exceeds the realistic form loss factor values and creates a very large flow resistance to reduce the flow entering and/or exiting the water rod. This provides a reasonable indication of whether the water rod behavior is significant during the LBLOCA, in terms of impacting quench front behavior and cladding temperatures within the main assembly channel.

An additional study was performed which investigated the impact of direct energy deposition to the coolant. 2.6% of the bundle power was assumed to be deposited directly into the coolant (all of which was assigned to the main assembly flow path in TRACE) in the results shown in the previous section. The additional case assumes 0% direct energy deposition, with all heat conducting and convecting from the

fuel rods instead. Although TRACE and CTF were consistent with regard to the direct energy deposition modeling (both applied 2.6% of heat directly to the coolant), this extra study was run simply to understand the direct energy deposition's effect for LBLOCA.

Figure 56 shows the outer surface PCT and quench front elevation results for the hot assembly in this sensitivity study. The constriction of water rod flow using a high form loss factor had very little effect on the behavior of the hot rod. It delayed the quench front propagation only slightly and led to a small outer surface PCT increase over the nominal case. The nominal water rod flow rate is a relatively small fraction of the total assembly flow, which contributed to this small impact. The solid temperatures of the water rod shell itself were also minimally impacted; although a difference in quench front behavior was seen, this did not translate to a large impact on the solid temperature itself.

The impact of direct heat deposition was also relatively minor for the hot assembly. The total linear heat rate in the assembly is small during the LBLOCA event because it reduces to decay heat levels several seconds into the event. However, the direct energy deposition could still potentially impact the quench front propagation because it impacts the heat flux leaving the cladding outer surface. This heat flux and its impact on the cladding and coolant conditions directly impacts the quenching behavior of the cladding surface. Nonetheless, the same total heat eventually reaches the coolant regardless of the fraction of heat which starts in the fuel rod, so the overall boiling rate should be similar and evidently the peak cladding temperature is similar as well, for either 0% or 2.6% direct heating.

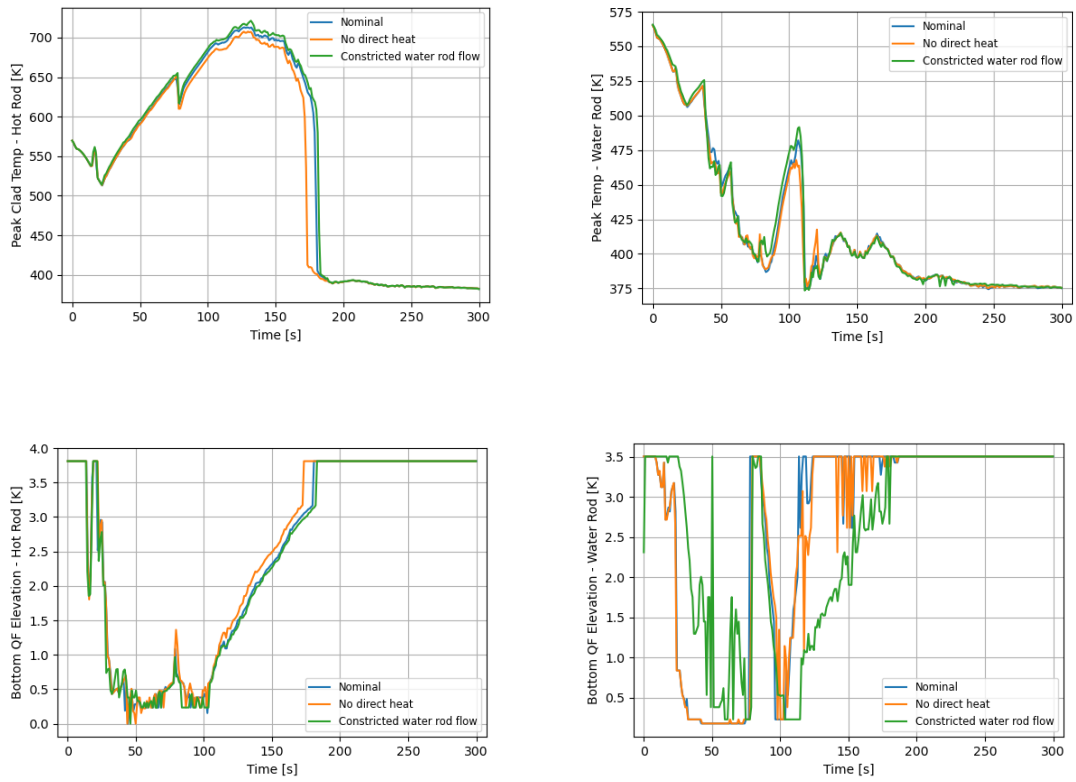

Figure 56. Results for the TRACE water rod flow constriction and direct energy deposition sensitivity studies for the hot assembly.

Figure 57 shows the results for the high-burnup assembly. Up until 80 s, the trend was similar to before, with little difference between the nominal case and the sensitivity cases, especially in the hot rod. However, after the large spike in the quench front elevation at 80 s, the hot rod outer surface PCT results for the sensitivity cases diverged from the nominal case. The exact cause of this quench front spike and the outer surface PCT divergence is not known, and it is unclear at this time whether it is based on a repeatable physical phenomenon or if numerical effects are at play. In any case, the water rod solid temperatures remained similar for all three runs despite the differences in hot rod behavior.

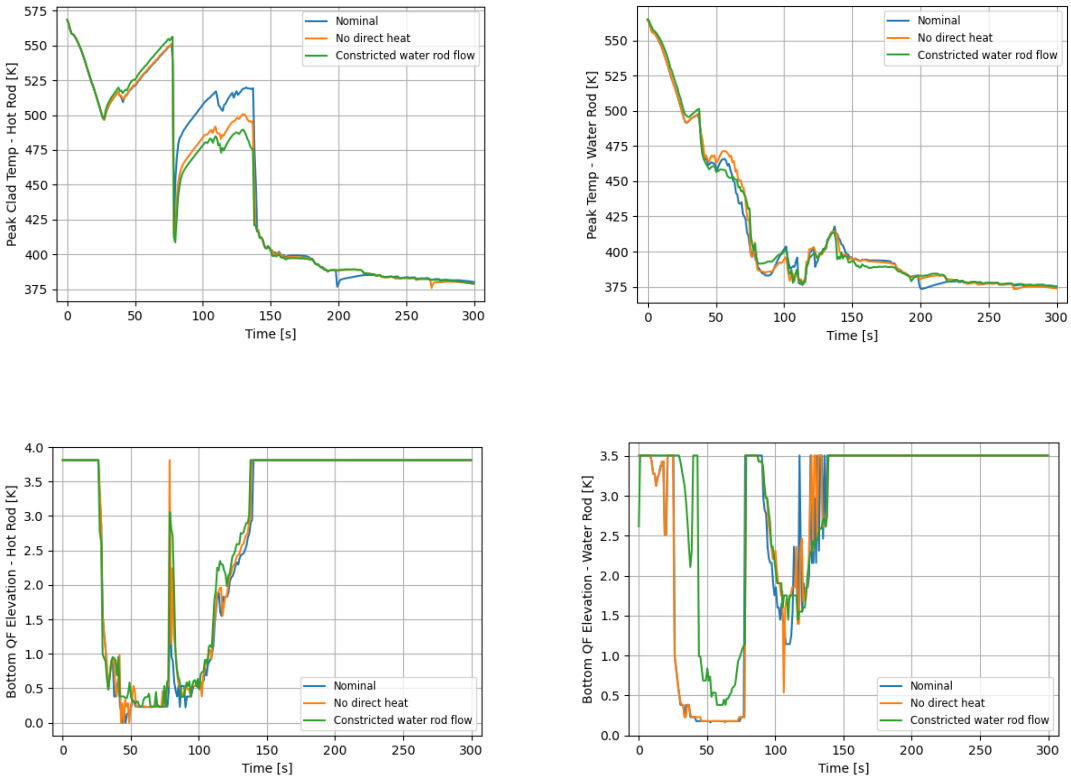

Figure 57. Results for the TRACE water rod flow constriction and direct energy deposition sensitivity studies for the high-burnup assembly.

8. CONCLUSIONS AND FUTURE WORK

The activities documented in this milestone report mark the completion of the development and demonstration of the VERA/BISON FFRD assessment framework for high-burnup BWR cores. Whereas FY24 work developed an initial limited capability that utilized a coarse mesh approach in the TRACE analysis and demonstrated only a few rods in the BISON analysis, the activities this year made use of the latest developments in TRACE and significantly expanded the BISON analysis. First, the TRACE mesh was refined from a four-channel model to a 195 channel model (one channel per assembly in the quarter core and 4 lumped channels in the remainder of the core). Additionally, a new feature that allows for capturing the full 3D power distribution provided by VERA in the TRACE model was utilized. In FY24 work, only one power profile per assembly could be utilized. Second, the BISON analysis was expanded from 8 rods to 945 rods that covered all burnup levels in the model. The main takeaways from the FFRD

analysis include the following summary, but it should be reiterated that these conclusions are for a representative core, and licensing basis assumptions or conservatisms were not utilized.

First, no rod burst was observed in any rods regardless of burnup level using either the CC or SRC models. A sensitivity analysis was also performed by artificially increasing the linear heat generation rate by up to 15% over nominal, which is consistent with the maximum level of disagreement observed between VERA and core measurements in previous work. Again, no rod burst was observed. To analyze rod burst behaviors, an earlier version of TRACE results with erroneous, unrealistically high temperatures in some peripheral, twice-burned assemblies was used. Unrealistically high values were used for the sole purpose of causing burst in some rods. Using these simulations, two rods were predicted to burst at 10% over-power, and seven burst at 15% over-power over the selected fuel rod population. A statistical analysis of these simulations showed positive correlations with burnup and cladding strain and negative correlations with fuel and cladding temperatures. The negative correlation with temperature was an unexpected result and should be investigated further in future work.

Second, an alternative aspect to this work was to perform a break size sensitivity analysis in the TRACE model. This type of activity will be necessary as the treatment of LOCA changes due to recent NRC draft rulemaking guidance. Small break LOCA (SBLOCA) analyses were performed which predicted cladding temperature increases that were bounded by the LBLOCA cladding temperatures for all break sizes studied; however, future improvements to the plant response assumptions during the SBLOCA could impact the predicted cladding response. It is noted that the PCTs evaluated in this study, for both LBLOCA and SBLOCA, are significantly lower than the PCTs in the Limerick-2 licensing basis. The current design basis PCT in Limerick-2 is 1375 K (2015 F) [16], which accounts for the impact of uncertainties and additional conservatisms not considered in the present TRACE analyses. The highest PCT in the TRACE studies was 830 K, which provides a reasonable indication of the PCT that may be expected under realistic assumptions and conditions. Furthermore, more break sizes need to be analyzed for both small and large break simulations to identify the limiting small and large break scenarios for more representative BISON analysis.

Another alternative aspect to this work was the performance of a benchmark between the CTF and TRACE T/H codes for analysis of BWR LOCA. The study revealed fairly consistent behavior in the fluid solution between the two codes; the void collapse rate is very consistent. At the location where PCT occurs, CTF always tends to predict higher PCT than TRACE; however, it also predicts a faster quench of the rod. This is consistent with the past benchmark study performed for PWRs. This study also marks the first application of using CTF for the blowdown phase of the LOCA. While the lumped benchmark was performed successfully, the rod-resolved benchmark was not possible due to issues with pressure spiking in the more refined CTF model during the blowdown. This indicates a need to further improve CTF stability before it will be widely applicable for rod-resolved full LOCA transient modeling.

Moving forward, there is a clear need for high-fidelity modeling and simulation as the industry moves towards increased enrichment and higher fuel utilization as a means of increasing power generation capability. This will support the Administration's Executive Order to facilitate 5 GW of power uprates at existing nuclear reactors by 2030 and will also improve the fuel cycle economy of the current fleet of LWRs. This framework should continue to be exercised utilizing the latest fuel performance models that support more accurate modeling of the most impactful phenomena to FFRD (e.g., hydrogen pickup). These analyses could then be used to support licensing decisions, benchmarking against more conservative industry methods, and identification of margin opportunities. In addition to the already identified improvement opportunities, future work should focus on the uncertainty of the multiphysics solution, work to improve validation of the methods against core data, and improve accuracy of the methods as required. Furthermore, once finalized, this infrastructure could easily be repurposed to investigate other major industry stakeholder ambitions such as time-at-temperature criteria development.

9. REFERENCES

[1] N. Capps, J. Hirschhorn, A. Wysocki, I. Greenquist, Assessment of the Effect of Prototypic High-Burnup Operating Conditions of Fuel Fragmentation, Relocation, and Dispersal Susceptibility, Oak Ridge National Laboratory, Oak Ridge, Tennessee, 2022.

[2] I. Greenquist, A. Wysocki, J. Hirschhorn, N. Capps, Multiphysics analysis of fuel fragmentation, relocation, and dispersal susceptibility–Part 1: Overview and code coupling strategies, Ann. Nucl. Energy 191 (2023) 109913. https://doi.org/10.1016/j.anucene.2023.109913.

[3] J. Hirschhorn, I. Greenquist, A. Wysocki, N. Capps, Multiphysics analysis of fuel Fragmentation, Relocation, and dispersal Susceptibility–Part 2: High-Burnup Steady-State operating and fuel performance conditions, Ann. Nucl. Energy 192 (2023) 109952. https://doi.org/10.1016/j.anucene.2023.109952.

[4] A. Wysocki, J. Hirschhorn, I. Greenquist, N. Capps, Multiphysics analysis of fuel fragmentation, relocation, and dispersal susceptibility–Part 3: Thermal hydraulic evaluation of large break LOCA under high-burnup conditions, Ann. Nucl. Energy 192 (2023) 109951. https://doi.org/10.1016/j.anucene.2023.109951.

[5] N. Capps, M. Asgari, A. Wysocki, I. Greenquist, S. Henderson, R.S. Jr, High Burnup BWR LOCA Burst Framework Development and Demonstration, Oak Ridge National Laboratory, Oak Ridge, Tennessee, 2024.

[6] N. Capps, R. Salko, M. Asgari, A. Wysocki, I. Greenquist, S. Henderson, B. Sarikaya, J. Tusar, I. Porter, High-burnup boiling water reactor steady-state operating conditions and fuel performance analysis, Ann. Nucl. Energy 215 (2025) 10. https://doi.org/10.1016/j.anucene.2025.111247.

[7] S. Bajorek, M. Gavrilas, C. Gingrich, J. Han, K. Hogan, J. Kelly, W. Krotiuk, N. Lauben, S. Lu, C. Murray, F. Odar, G. Rhee, M. Rubin, S. Smith, J. Staudenmeier, J. Uhle, W. Wang, K. Welter, J. Han, V. Klein, W. Burton, J. Danna, J. Jolicoeur, S. Basu, I. Madni, S. Marshall, A. Velazquez, P. Kadambi, D. Bessette, M. Bennet, M. Salay, A. Ireland, W. Macon, F. Eltawila, Y. Guan, D. Ebert, D. Du, T. Fang, W. He, M. Straka, D. Palmrose, Jones, J. Mahaffy, M. Trujillo, M. Jelinek, M. Lazor, B. Hansell, J. Watson, M. Meholic, B. Aktas, C. Amoruso, D. Barber, M. Bolander, D. Caraher, C. Delfino, D. Fletcher, D. Larson, S. Lucas, G. Mortensen, V. Palazov, D. Prelewicz, R. Shumway, R. Tompot, D. Wang, J. Spore, B. Boyack, S. Dearing, J. Durkee, J. Elson, P. Giguere, R. Johns, J. Lime, J.-C. Lin, D. Pimentel, T. Downar, M. Miller, J. Gan, H. Joo, Y. Xu, T. Kozlowski, D. Jung Lee, R. Herrero, J.H. Jeong, C.W. Huh, A.D. Shin, TRACE V5.0 Theory Manual: Field Equations, Solution Methods, and Physical Models, (n.d.). https://www.nrc.gov/docs/ML1200/ML120060218.pdf.

[8] R.L. Williamson, J.D. Hales, S.R. Novascone, G. Pastore, K.A. Gamble, B.W. Spencer, W. Jiang, S.A. Pitts, A. Casagranda, D. Schwen, A.X. Zabriskie, A. Toptan, R. Gardner, C. Matthews, W. Liu, H. Chen, BISON: A Flexible Code for Advanced Simulation of the Performance of Multiple Nuclear Fuel Forms, Nucl. Technol. 207 (2021) 954–980. https://doi.org/10.1080/00295450.2020.1836940.

[9] K.A. Gamble, A. Toptan, P.-C.A. Simon, D.J. van Wasshenova, J.D. Hales, Enabling BWR fuel rod analysis in the BISON fuel performance code, J. Nucl. Mater. 616 (2025) 25. https://doi.org/10.1016/j.jnucmat.2025.156038.

[10] High Burnup Lead Use Assembly (HBLUA) Information Report for Limerick 2, Global Nuclear Fuel, 2021.

[11] D.A. Powers, R.O. Meyer, Cladding Swelling and Rupture Models for LOCA Analysis, U.S. Nuclear Regulatory Commission, Washington, DC, 1980.

[12] F.J. Erbacher, H.J. Neitzel, H. Rosinger, H. Schmidt, K. Weihr, Burst Criterion of Zircaloy Fuel Claddings in a Loss-of-Coolant Accident, in: Zircon. Nucl. Ind., ASTM International, 1982: pp. 271–282.
[13] V. Di Marcello, A. Schubert, J. van de Laar, P. Van Uffelen, The TRANSURANUS mechanical model for large strain analysis, Nucl. Eng. Des. 276 (2014) 19–29. https://doi.org/10.1016/j.nucengdes.2014.04.041.
[14] W. Wagner, A. Pruß, The IAPWS Formulation 1995 for the Thermodynamic Properties of Ordinary Water Substance for General and Scientific Use, J. Phys. Chem. Ref. Data 31 (2002) 387–535. https://doi.org/10.1063/1.1461829.
[15] R. Salko, A. Wysocki, B. Hizoum, N. Capps, A study on the impact of using a subchannel resolution for modeling of large break loss of coolant accidents, Ann. Nucl. Energy 207 (2024) 12. https://doi.org/10.1016/j.anucene.2024.110716.
[16] D.P. Helker, Limerick Generating Station, Units 1 and 2 - 10 CFR 50.46 Annual Report, (2024). https://www.nrc.gov/docs/ML2430/ML24303A278.pdf.